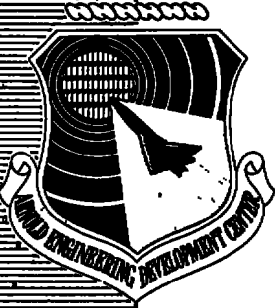


AEDC-TR-76-28

cy.1

**ARCHIVE COPY  
DO NOT LOAN**



**HEAT-TRANSFER TESTS  
ON THE ROCKWELL INTERNATIONAL SPACE  
SHUTTLE ORBITER WITH BOUNDARY-LAYER TRIPS (OH-54)**

**VON KÁRMÁN GAS DYNAMICS FACILITY  
ARNOLD ENGINEERING DEVELOPMENT CENTER  
AIR FORCE SYSTEMS COMMAND  
ARNOLD AIR FORCE STATION, TENNESSEE 37389**

**May 1976**

**Final Report for Period October 1974 — September 1975**

Approved for public release; distribution unlimited.

Property of U. S. Air Force  
AEDC LIBRARY  
F40600-75-C-0001

Prepared for

**NATIONAL AERONAUTICS AND SPACE ADMINISTRATION (JSC)  
HOUSTON, TEXAS 77058**



## NOTICES

When U. S. Government drawings specifications, or other data are used for any purpose other than a definitely related Government procurement operation, the Government thereby incurs no responsibility nor any obligation whatsoever, and the fact that the Government may have formulated, furnished, or in any way supplied the said drawings, specifications, or other data, is not to be regarded by implication or otherwise, or in any manner licensing the holder or any other person or corporation, or conveying any rights or permission to manufacture, use, or sell any patented invention that may in any way be related thereto.

Qualified users may obtain copies of this report from the Defense Documentation Center.

References to named commercial products in this report are not to be considered in any sense as an endorsement of the product by the United States Air Force or the Government.

This report has been reviewed by the Information Office (OI) and is releasable to the National Technical Information Service (NTIS). At NTIS, it will be available to the general public, including foreign nations.

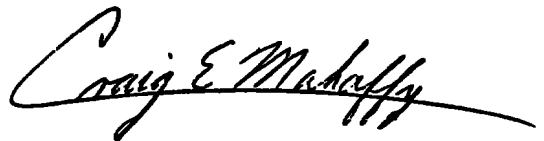
## APPROVAL STATEMENT

This technical report has been reviewed and is approved for publication.

FOR THE COMMANDER



CARL J. SCHULZE  
Major, USAF  
Chief Air Force Test Director, VKF  
Directorate of Test



CRAIG E. MAHAFFY  
Colonel, USAF  
Director of Test

# UNCLASSIFIED

REPORT DOCUMENTATION PAGE		READ INSTRUCTIONS BEFORE COMPLETING FORM
1 REPORT NUMBER <b>AEDC-TR-76-28</b>	2 GOVT ACCESSION NO.	3 RECIPIENT'S CATALOG NUMBER
4. TITLE (and Subtitle) <b>HEAT-TRANSFER TESTS ON THE ROCKWELL INTERNATIONAL SPACE SHUTTLE ORBITER WITH BOUNDARY-LAYER TRIPS (OH-54)</b>		5. TYPE OF REPORT & PERIOD COVERED <b>Final Report - October 1974 - September 1975</b>
		6. PERFORMING ORG. REPORT NUMBER
7 AUTHOR(s)  <b>D. B. Carver - ARO, Inc.</b>		8. CONTRACT OR GRANT NUMBER(s)
		9. PERFORMING ORGANIZATION NAME AND ADDRESS <b>Arnold Engineering Development Center (XO) Air Force Systems Command Arnold Air Force Station, Tennessee 37389</b>
11 CONTROLLING OFFICE NAME AND ADDRESS <b>National Aeronautics and Space Administration (JSC/ES3), Houston, Texas 77058</b>		10 PROGRAM ELEMENT, PROJECT, TASK AREA & WORK UNIT NUMBERS  <b>Program Element 921E</b>
		12. REPORT DATE
14 MONITORING AGENCY NAME & ADDRESS (if different from Controlling Office)		13. NUMBER OF PAGES  <b>40</b>
		15. SECURITY CLASS. (of this report)  <b>UNCLASSIFIED</b>
		15a. DECLASSIFICATION/DOWNGRADING SCHEDULE  <b>N/A</b>
16 DISTRIBUTION STATEMENT (of this Report)  <b>Approved for public release; distribution unlimited.</b>		
17. DISTRIBUTION STATEMENT (of the abstract entered in Block 20, if different from Report)  <i>2. Reentry Vehicle - - Boundary Layer Trips</i>		
18 SUPPLEMENTARY NOTES  <b>Available in DDC</b> <i>3. Reentry Vehicle - - Heat Transfer</i>		
19. KEY WORDS (Continue on reverse side if necessary and identify by block number) <b>aerodynamic heating</b> <b>heat transfer</b> <b>reentry vehicles</b> <b>photographic techniques</b> <b>spacecraft</b>  <i>orbit shuttle</i> <i>boundary layer transition</i>		
20. ABSTRACT (Continue on reverse side if necessary and identify by block number) <b>Aerothermodynamic transition tests on a model of the forward half of the Rockwell International Space Shuttle Orbiter Configuration 140C were conducted at Mach number 8. Phase-change paint was used to determine the aerodynamic heating rates on the windward side of Orbiter models during simulated atmospheric reentry. The majority of the data was obtained using spherical trip elements of varying sizes at three different axial stations along the model to determine the effect of roughness size and location on boundary-</b>		

# UNCLASSIFIED

# UNCLASSIFIED

## 20. ABSTRACT (Continued)

layer transition. Additional data were taken with models which had scale indentations that simulated external tank attachment rings, nose wheel well doors, and a surface insulation interface gap. Data were taken over an angle-of-attack range from 20 to 40 deg at free-stream Reynolds numbers, based on the total Orbiter scaled length, from 3.2 to 16.1 million. Typical heat-transfer data are presented to illustrate boundary-layer transition locations and sensitivities to test variables.

## PREFACE

The work reported herein was conducted by the Arnold Engineering Development Center (AEDC), Air Force Systems Command (AFSC), at the request of the National Aeronautics and Space Administration (NASA/JSC) for Rockwell International Space Division, Downey, California, under Program Element 921E. The results were obtained by ARO, Inc. (a subsidiary of Sverdrup & Parcel and Associates, Inc.), contract operator of AEDC, AFSC, Arnold Air Force Station, Tennessee, under ARO Project Number V41B-82A. The author of this technical report was D. B. Carver, ARO, Inc. The test was performed intermittently over the period from October 1974 through September 1975. The final data package was completed on October 2, 1975, and the manuscript (ARO Control No. ARO-VKF-TR-75-165) was submitted for publication on December 1, 1975.

The author wishes to express his gratitude to Mr. F. K. Hube and Mr. W. R. Martindale for their assistance during the planning and testing phases of this program and to Dr. A. W. Mayne, Jr., for performing the theoretical computations.

## CONTENTS

	<u>Page</u>
1.0 INTRODUCTION . . . . .	5
2.0 APPARATUS	
2.1 Wind Tunnel . . . . .	5
2.2 Models . . . . .	5
2.3 Instrumentation . . . . .	6
3.0 PROCEDURES	
3.1 Test Conditions . . . . .	7
3.2 Test Procedures . . . . .	8
3.3 Data Reduction . . . . .	8
3.4 Precision of Measurements . . . . .	9
4.0 RESULTS AND DISCUSSION . . . . .	10
5.0 SUMMARY OF RESULTS . . . . .	13
REFERENCES . . . . .	14

## ILLUSTRATIONS

### Figure

1. Tunnel B . . . . .	15
2. Model Photographs . . . . .	16
3. Sketch of the Orbiter Forebody Models . . . . .	19
4. Trip Ring Photograph . . . . .	20
5. Photograph of the Smooth Trip Ring Modified to Simulate the External Tank Attachment Ring . . . . .	21
6. Photograph of the Paint Stripe Model . . . . .	22
7. Typical Shadowgraphs, 0.031-in.-diam Spheres at $X_k/L = 0.168$ , $Re_{\infty,L} = 6.5 \times 10^6$ . . . . .	23
8. Phase-Change Paint Photographs of the Mid-Station Trip Model with a Smooth Trip Ring Installed, $Re_{\infty,L} = 12.9 \times 10^6$ , $\alpha = 30$ deg . . . . .	24
9. Phase-Change Paint Photographs of an External Tank Attachment Ring Configuration ( $r_1 = 0.063$ in., $d = 0.050$ in.) $Re_{\infty,L} = 12.9 \times 10^6$ , $\alpha = 30$ deg . . . . .	25
10. Phase-Change Paint Photographs of a Trip Model, 0.031-in.-diam Spheres at $X_k/L = 0.110$ , $Re_{\infty,L} = 8.6 \times 10^6$ , $\alpha = 30$ deg . . . . .	26
11. Photographs of the Effect of Angle of Attack for a Constant Melt Line Heat-Transfer Coefficient, $h/h_{ref} = 0.27$ , 0.020-in.-diam Spheres at $X_k/L = 0.168$ , $Re_{\infty,L} = 12.9 \times 10^6$ . . . . .	27

<u>Figure</u>	<u>Page</u>
12. Determination of the Laminar Heat-Transfer Distribution along the Windward Centerline . . . . .	28
13. Effect of Reynolds Number on the Windward Centerline Heat-Transfer Distribution, 0.031-in.-diam Spheres at $X_k/L = 0.110$ , $\alpha = 30$ deg . . . . .	31
14. Determination of Trip Effectiveness, 0.031-in.-diam Spheres at $X_k/L = 0.110$ , $\alpha = 30$ deg . . . . .	32
15. Effect of the Copper Nose on the Windward Centerline Temperature Distribution, $Re_{\infty,L} = 8.6 \times 10^6$ , $\alpha = 30$ deg . . . . .	33

**TABLES**

1. Trip Sphere Sizes Tested . . . . .	34
2. External Tank Attachment Ring Dimensions . . . . .	34
3. Summary of Test Data . . . . .	35
4. Model Material Thermophysical Properties . . . . .	38

NOMENCLATURE . . . . .	39
------------------------	----

## 1.0 INTRODUCTION

The test described herein (designated OH-54 by Rockwell International) was designed as a parametric study of boundary-layer transition and heating rates on the windward side of the 140C Space Shuttle Orbiter Configuration. Various trip devices were used at different axial stations along the model: (1) spherical elements, (2) external tank attachment ring simulations, (3) surface insulation interface gap, and (4) simulated nose-wheel well doors. To provide adequate definition of heating rate distributions, it was necessary to test models as large as possible. The testing of a 4-percent model scale was made feasible by simulating only the forward half of the Orbiter ( $L/2 = 25.8$  in.).

The test was conducted using the phase-change paint technique to obtain heat-transfer data. The data were obtained in Hypersonic Wind Tunnel (B) of the von Kármán Gas Dynamics Facility (VKF) at a nominal Mach number of 8. Angle of attack was varied from 20 to 40 deg at free-stream Reynolds numbers from 3.2 to 16.1 million based on the scaled Orbiter's full length ( $L = 51.6$  in.).

## 2.0 APPARATUS

### 2.1 WIND TUNNEL

Tunnel B is a closed-circuit hypersonic wind tunnel with a 50-in.-diam test section. Two axisymmetric contoured nozzles are available to provide Mach numbers of 6 and 8, and the tunnel may be operated continuously over a range of pressure levels from 20 to 300 psia at  $M_{\infty} = 6$  and 50 to 900 psia at  $M_{\infty} = 8$ , with air supplied by the VKF main compressor plant. Stagnation temperatures sufficient to avoid air liquefaction in the test section (up to  $1,350^{\circ}\text{R}$ ) are obtained through the use of a natural gas fired combustion heater. The entire tunnel (throat, nozzle, test section, and diffuser) is cooled by integral, external water jackets. The tunnel is equipped with a model injection system, which allows removal of the model from the test section while the tunnel remains in operation. A more complete description of the tunnel is presented in Ref. 1. The tunnel assembly is shown in Fig. 1.

### 2.2 MODELS

The model were 0.04-scale models of the forward half (forebody) of the Rockwell International Space Shuttle Orbiter 140C. Contours of the models are defined by Rockwell drawing VL70-000140C. Lockheed Missiles and Space Company (LMSC) of Huntsville, Alabama, subcontractors for model fabrication, cast the models from a proprietary epoxy material (Material LH), which has a low thermal diffusivity and relatively high strength. The models were cast as a one-piece shell with a nominal wall thickness of 1 in. and



then filled with foam. Samples of the same batch of epoxy used to cast the models were analyzed by LMSC to determine the thermophysical properties (density, specific heat, and conductivity) which were necessary for data reduction. Photographs and details of the models and model components are shown in Figs. 2 through 6.

The majority of the test was devoted to testing of boundary-layer trip models. Three separate models were used, each with the trip located at a different axial station along the model (trips at  $X_k/L = 0.052, 0.110, \text{ and } 0.168$ ). Trip model photographs are presented in Fig. 2 and the basic model geometry is shown in Fig. 3. The three trip models were modified to incorporate copper nose pieces (see Fig. 2b) after the first test entry. The nose pieces were pure copper, plated with 0.005 in. of nickel for hardness. The copper served as a heat sink, thus keeping the nosetip temperature relatively constant throughout a group of data and, in addition, allowed longer test runs without fear of model damage as a result of overheating. Thermocouples were located along the bottom centerline of the copper nose pieces to monitor the nosetip temperature rise during a test run.

The transition devices were mounted on 1/4-in.-wide stainless steel inserts (trip rings) that fit the model contour. Stainless steel balls were spot welded to the rings with a spacing of four ball diameters center to center. Extreme care was taken during the welding process to prevent deformation of the balls such that all the balls on a trip ring were perfect spheres of equal diameter within  $\pm 2$  percent of the nominal diameter. Individual trip rings were provided with ball diameters of 0.000 (smooth insert), 0.015, 0.020, 0.025, 0.031, and 0.039 in. A photograph of a trip ring is presented in Fig. 4 and a complete listing of ball sizes tested at each axial station is given in Table 1. The smooth trip ring for the mid-station ( $X_k/L = 0.110$ ) trip model was modified to accept various inserts to simulate external tank (ET) attachment ring configurations. The insert formed an annulus with a total diameter of 0.225 in. A photograph of the ring and inserts is presented in Fig. 5, and the annulus dimensions are listed in Table 2.

Other models tested include a smooth model, a protuberance model with simulated nose wheel well doors, and a model with a simulated interface gap between two insulation materials designated as the Reusable Carbon-Carbon/High Temperature Reusable Surface Insulation (RCC-HRSI) interface gap model. The location of the nose wheel well doors is shown in Fig. 3. The RCC-HRSI interface gap was simulated by a 0.040-in.-wide by 0.080-in.-deep circumferential groove located at model station  $X/L = 0.020$  in.

## 2.3 INSTRUMENTATION

Tunnel B stilling chamber pressure is measured with a 100- or 1,000-psia transducer referenced to a near vacuum. Based on periodic comparisons with secondary standards, the uncertainty (a bandwidth which includes 95 percent of residuals) of the transducers

is estimated to be within  $\pm 0.1$  percent of reading or  $\pm 0.06$  psi whichever is greater for the 100-psid range and  $\pm 0.1$  percent of reading or  $\pm 0.5$  psi whichever is greater for the 1,000-psid range. Stilling chamber temperature measurements are made with Chromel<sup>®</sup>-Alumel<sup>®</sup> thermocouples which have an uncertainty of  $\pm(1.5^{\circ}\text{F} + 0.375$  percent of reading) based on repeat calibrations.

Model-sting deflections were measured with a strain gage attached to the model support sting. Prior to the test, static loads were applied at the expected center-of-pressure location to determine the gage calibration with respect to the deflection angle. The deflection calculation was incorporated into the data reduction program. This procedure made it possible to preset the desired angle of attack with an uncertainty of approximately  $\pm 0.2$  deg.

As many as nine Chromel<sup>®</sup>-Constantan thermocouples were located on the model for measurement of the copper nosetip temperature.

### 3.0 PROCEDURES

#### 3.1 TEST CONDITIONS

The tests were conducted in Tunnel B at a nominal Mach number of 8 over a free-stream unit Reynolds number range from 0.75 to 3.75 million/ft. Data were taken at model angle-of-attack values of 20, 30, 35, and 40 deg. The nominal tunnel test conditions are listed below, while a complete test summary is presented in Table 3.

$M_{\infty}$	$p_o$ , psia	$T_o$ , °R	$h_{ref}$ , Btu/ft <sup>2</sup> -sec-°R	$Re_{\infty} \times 10^{-6}$ , ft <sup>-1</sup>
7.93	155	1,270	0.014	0.75
7.94	210	1,275	0.016	1.00
7.95	265	1,280	0.018	1.25
7.96	320	1,290	0.020	1.50
7.97	375	1,295	0.022	1.75
7.98	425	1,300	0.023	2.00
7.98	490	1,310	0.025	2.25
7.99	555	1,320	0.026	2.50
7.99	610	1,325	0.027	2.75
7.99	670	1,330	0.029	3.00
8.00	735	1,330	0.030	3.25
8.00	800	1,335	0.031	3.50
8.00	850	1,340	0.032	3.75

## 3.2 TEST PROCEDURES

After the completion of the camera installations and prior to the test, photographs were taken of the "paint stripe" model (see Fig. 6) at each of the model test attitudes. These photographs provided the model reference coordinates necessary for the data reduction.

The models were installed in an inverted position to facilitate photographic coverage of the windward surface (see Fig. 2c). Prior to each run, the model was cleaned and cooled with alcohol and then spray painted with a phase-change paint (Tempilaq®). Only the windward surface was painted since the area of interest was transition location on the windward surface. All painting was performed in the injection tank to minimize damage (knocking off trip spheres) to the trip-rings. A mask was used to prevent painting of the trip-rings. The model initial surface temperature was measured and the model was then injected into the airstream for approximately 25 sec. During this time, the model surface temperature rise produced isotherm melt lines. The progress of the melt lines was photographed with a 70-mm sequence camera at the rate of one frame per second. A video system was used to provide an "on-line" instant playback for use in establishing a rough estimate of transition location, from which the next set of test conditions (angle and Reynolds number) was determined. Generally, one model was tested per test-shift, and one trip-ring was tested until the test matrix on that configuration was complete. Another trip-ring (different sphere size) was installed only upon completion of the test matrix in order to minimize damage to the trip-ring. One shadowgraph photograph was taken per group to monitor the flow conditions. Selected shadowgraphs are presented in Fig. 7.

During each run, the tunnel stagnation conditions and the time of each picture were recorded on magnetic tape as well as the model initial temperature, the phase-change paint temperature ( $T_{pc}$ ), and the model angle of attack. Nostip temperatures were also recorded on those models which had thermocouples. These data were reduced using the standard VKF data reduction program to provide heat-transfer parameters to correspond with the photographed melt lines.

## 3.3 DATA REDUCTION

Reduction of phase-change paint data is based on the assumption that the model wall heating can be represented (thermally) by a semi-infinite slab (Refs. 2 and 3). A material with a low thermal diffusivity is necessary for this assumption to be valid for reasonable model wall thicknesses and testing times.

The phase-change paint technique of obtaining heat-transfer data uses a fusible coating which changes from an opaque solid to a transparent liquid (i.e., it melts) at a specified temperature ( $T_{pc}$ ). The demarcations between melted and unmelted paint (melt lines) are model surface isotherms and are used to evaluate the aerodynamic heating. Tempilaq paint was used as the phase-change coating for these tests. The calibrated melting points of the paints used were 150, 169, 175, 200, 250, 275, 300, 350, 388, 400, and 413°F. A more complete description of the phase-change paint technique is presented in Ref. 3.

Data reduction of the melt line photographs was accomplished by making tracings of these isothermal lines for various times during the test run. The lines of each of these tracings were related to corresponding aerodynamic heat-transfer coefficients ( $h$ ) by applying the semi-infinite slab heat equation, given below:

$$\left( \frac{T_{pc} - T_i}{T_{aw} - T_i} \right) = 1 - e^{\beta^2} \cdot \operatorname{erfc} \beta$$

where

$$\beta = \frac{h\sqrt{\Delta t}}{\sqrt{wc_p k}}$$

and

$$\Delta t = \text{time of heating}$$

The lumped material thermophysical property  $\sqrt{wc_p k}$  was a function of temperature (see Table 4). The heat-transfer coefficients were computed for an assumed adiabatic temperature ( $T_{aw}$ ) of  $T_o$ . The Fay-Riddell stagnation point heat-transfer coefficient (Ref. 4) ( $h_{ref}$ ), based on a 0.04-ft-radius sphere, was used to normalize the computed aerodynamic heat-transfer coefficients. (The radius of this hypothetical sphere would be 1 ft at corresponding Orbiter full-scale conditions.)

### 3.4 PRECISION OF MEASUREMENTS

#### 3.4.1 Test Conditions

Uncertainties of the basic tunnel flow parameters ( $p_o$ ,  $T_o$ , and  $M_\infty$ ) were estimated from repeat calibrations of the instruments and from repeatability and uniformity of the test section flow during tunnel calibrations. The individual contributions of these uncertainties were used to compute the uncertainties in the other parameters dependent on these by means of the Taylor Series method of error propagation.

<u>Parameter</u>	<u>Uncertainty (<math>\pm</math>), percent</u>
$P_o$	0.5
$T_o$	0.5
$M_\infty$	0.3
$h_{ref}$	0.8
$Re_\infty$	1.2

### 3.4.2 Data

An accurate estimate of the precision of phase-change paint data is hampered by the fact that an observer must determine the location of the melt line (Ref. 5). For the results presented in this report, only uncertainties attributable to the measured parameters are considered. The parameters needed for the solution of the equation for the heat-transfer coefficient ( $h$ ) are  $T_o$ ,  $T_{pc}$ ,  $T_i$ ,  $\sqrt{wc_p k}$ , and  $\Delta t$ . The nominal uncertainties in these specific parameters are summarized below:

<u>Parameter</u>	<u>Uncertainty, percent</u>
$\Delta t$	$\pm 1.0$
$\sqrt{wc_p k}$	$\pm 10.0$
$T_i$	$\pm 0.5$
$T_o$	$\pm 0.5$
$T_{pc}$	$\pm 0.5$

Combining the above measurement uncertainties using the Taylor Series method of error propagation yields

for  $T_{pc} \leq 200^\circ\text{F}$ ,  $h$  uncertainty  $\approx \pm 13$  percent

for  $T_{pc} > 200^\circ\text{F}$ ,  $h$  uncertainty  $\approx \pm 11$  percent

The above uncertainties are based solely on the measured parameters that were used in the semi-infinite slab equation. Conduction errors could require that the heat-transfer levels be adjusted upward; however, corrections would necessitate additional assumptions.

## 4.0 RESULTS AND DISCUSSION

The aerodynamic heating rates generated by a turbulent boundary layer may be several times greater than that for laminar flow at the same flight condition. Requirements of

the thermal protection system necessary for the windward surface of the orbiter vehicle will, therefore, depend largely on where and when transition from laminar to turbulent flow occurs. The tests reported herein were designed to determine the effects that various roughness elements may have on premature flow transition. The results presented are typical of the data obtained.

Selected phase-change paint photographs are presented in Figs. 8 through 11. The noted heat-transfer rate applies to the melt line only. The melted areas indicate heat-transfer rates greater than the noted value, and the unmelted areas indicate heat-transfer rates lower than the noted value. Natural transition (no trip) on a smooth model is exhibited in Fig. 8. The melt line progresses smoothly with time from both upstream and downstream directions, and the last point to melt (if the model had been allowed to remain in the tunnel) would be at the beginning of transition. The blemishes noted were caused by slight nonuniformities in the model properties incurred during the model casting process. The effect of a small longitudinal crack near the base of the model is also readily apparent (top photo, Fig. 8).

The shape of the turbulent wedge generated by an external tank (ET) attachment ring configuration is illustrated in Fig. 9. The photographs show the heat-transfer distribution to be relatively constant within the turbulent wedge (almost simultaneous melt), which is typical of an effective trip. Figure 10 is an example of the melt pattern exhibited for an effective spherical element trip. Each of the balls generates a turbulent wake as evidenced by the streaks immediately aft of the trip ring. The merging of these streaks represents the development of uniform turbulent flow. The unmelted spike noted in Fig. 10 was caused by a missing trip sphere.

Photographs of the melt pattern at a constant melt line heat-transfer rate ( $h/h_{ref} = 0.27$ ) for 20-, 30-, and 40-deg angles of attack are presented in Fig. 11 for the mid-station (0.031-in.-diam spheres at  $X_k/L = 0.110$ ) trip model. Two basic observations are possible with these photographs. First, the overall heat-transfer rate is significantly higher at the higher angles of attack. Second, the spherical trip elements become more effective as a result of the thinner boundary layer at the higher angles of attack.

A thorough evaluation of transition requires that the laminar and turbulent heat-transfer distributions be known for each test condition. The laminar distributions along the windward centerline shown in Fig. 12 were determined by fairing of low Reynolds number data from essentially smooth models. Data from an earlier test on a smooth thin-skin model (Ref. 6) provided a complete definition of the laminar distributions. The agreement between the paint data (shaded symbols) and the thin-skin data (open symbols) is considered good. Paint data were not obtained on a smooth model at  $\alpha = 20$  deg for

the lower Reynolds numbers; therefore, the data from the RCC-HRSI interface gap model is presented for comparison with the thin-skin data. Comparison of the data for the smooth model and the RCC-HRSI interface gap model at  $\alpha = 40$  deg shows the RCC-HRSI interface gap to have no measurable effect on transition. As expected, the laminar heating rate distributions for various free-stream Reynolds numbers are well correlated by the Fay-Riddell reference level ( $h_{ref}$ ). For the two lower Reynolds numbers, laminar flow existed along the entire length of the body for all angles of attack.

Windward centerline heat-transfer data, for the mid-station trip configuration with 0.031-in.-diam spheres, are presented in Fig. 13 to illustrate the effect of Reynolds number on boundary-layer transition. The beginning of transition is readily obtained for the lower free-stream Reynolds number ( $Re_{\infty,L} = 4.4 \times 10^6$ ). Definition of the beginning of transition for the higher Reynolds numbers would require additional data at the lower heat-transfer levels which would have required repeating the same test conditions with a lower phase-change paint temperature.

The theoretical turbulent heat-transfer rate distributions shown in Fig. 13 were obtained from calculations using the method of Patankar and Spaulding (Ref. 7), as modified by Mayne and Dyer (Ref. 8), which uses an axisymmetric body at zero incidence to represent the vehicle geometry. The required inviscid computational data were obtained using the method of Ref. 9. The computations (which existed prior to this test program) were performed using a hyperboloid to approximate the windward surface geometry of the 139 Shuttle Orbiter configuration at  $\alpha = 30$  deg. The windward centerline geometry of the 140C Shuttle Orbiter configuration is reasonably close to that of the 139; therefore, the theory should provide a good estimate of the turbulent heat-transfer rates.

Comparison of the data with the theoretical rates (see Fig. 13) indicates reasonable agreement (within 15 percent). The locations of the ends of transition noted in Fig. 13 and used in subsequent analysis were obtained from the intersections of the slopes (hand fit) of transitional data with the fully turbulent heat-transfer rates determined from the data. Data at the two highest Reynolds numbers show the heat-transfer rate to "overshoot" the fully turbulent level, which is typical of an "effective" trip. The reversal of the data trend with Reynolds number between  $Re_{\infty,L} = 5.4 \times 10^6$  and  $6.5 \times 10^6$  is unexplained. It is possible that an unidentified roughness, such as a granular paint application, could have caused premature transition in the  $Re_{\infty,L} = 5.4 \times 10^6$  case.

A simple method of evaluating trip effectiveness is to plot the transition location ( $X_t/L$ ) vs  $Re_{\infty,L}$  as illustrated in Fig. 14. The deviation of the "tripped" data from the natural transition data (smooth model) is quite pronounced. An assumed variation in the natural transition data (see Ref. 2 for example):

$$X_t/L \approx (Re_{\infty,L})^{-0.8}$$

provides a trend for comparison to "tripped" data. The Reynolds number at which the trip becomes "effective" is shown as the "knee" location in Fig. 14. As can be seen, the trips became "effective" at a free-stream Reynolds number of about 10 million for this particular case.

A test technique problem common to phase-change paint tests is that the model nose temperature rises rapidly during a test run. This is of particular concern for boundary-layer trip evaluation tests since the boundary-layer thickness increases with temperature. For these tests, the copper nose piece, located forward of the trip ring, maintained an essentially constant temperature throughout a test run, thus providing a relatively constant boundary-layer thickness approaching the trip. The effectiveness of the copper nose is illustrated in Fig. 15 by comparing measured temperatures with those expected if the copper noses did not exist. Also, longer run times were possible with the copper nose without fear of model damage from overheating.

## 5.0 SUMMARY OF RESULTS

Phase-change paint heat-transfer tests were conducted to evaluate the effects of various roughness elements on boundary-layer transition on the forward half of the Rockwell International 140C Configuration Space Shuttle Orbiter at simulated reentry conditions. The Reynolds number, based on the total model scaled length, was varied from 3.2 million to 16.1 million over an angle-of-attack range from 20 to 40 deg at a Mach number of 8. From the data presented, the following conclusions were reached:

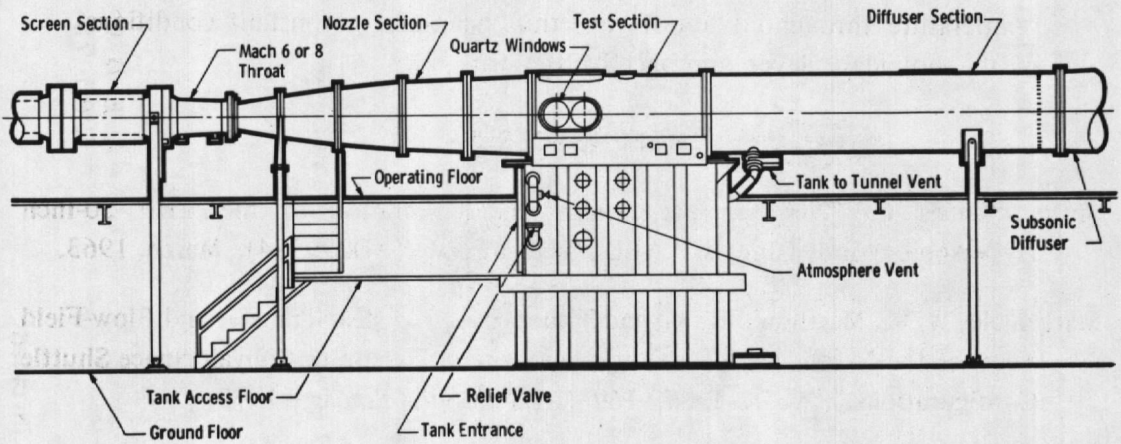
1. The Reusable Carbon-Carbon/High Temperature Reusable Surface Insulation (RCC/HRSI) interface gap had no measurable effect on boundary-layer transition at  $\alpha = 40$  deg,  $Re_{\infty,L} = 8.6 \times 10^6$ .
2. The spherical trip elements were clearly effective in tripping the boundary layer.
3. Definition of end-of-transition along the windward centerline was possible from the data, whereas definition of beginning-of-transition would require additional data at the same test conditions with a lower paint temperature.
4. The laminar heating rates agreed with previous data and were well correlated by theory, and the turbulent heating rates obtained with trips agreed with calculated values within 15 percent.



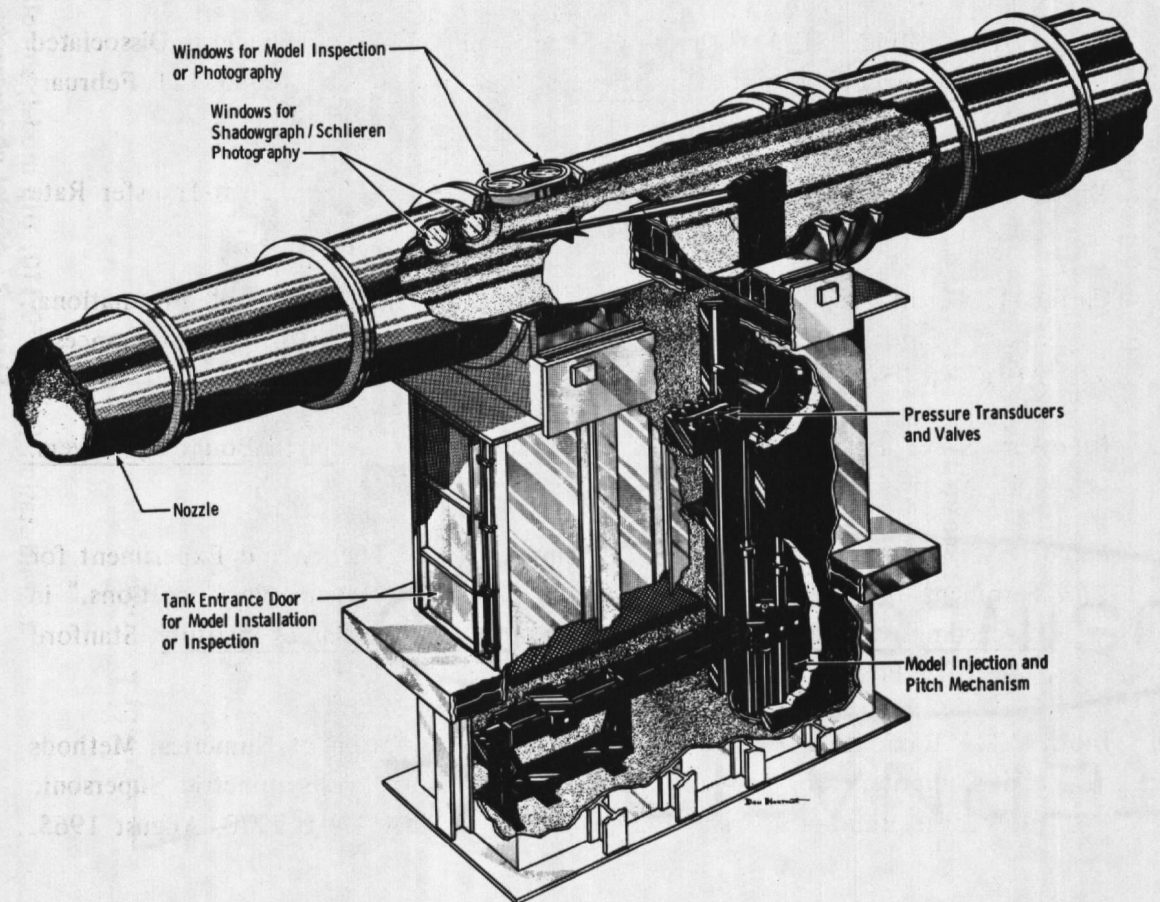
5. The copper nose was effective in maintaining an essentially constant temperature throughout a test run, thus maintaining constant conditions in the boundary layer approaching the trip ring.

### REFERENCES

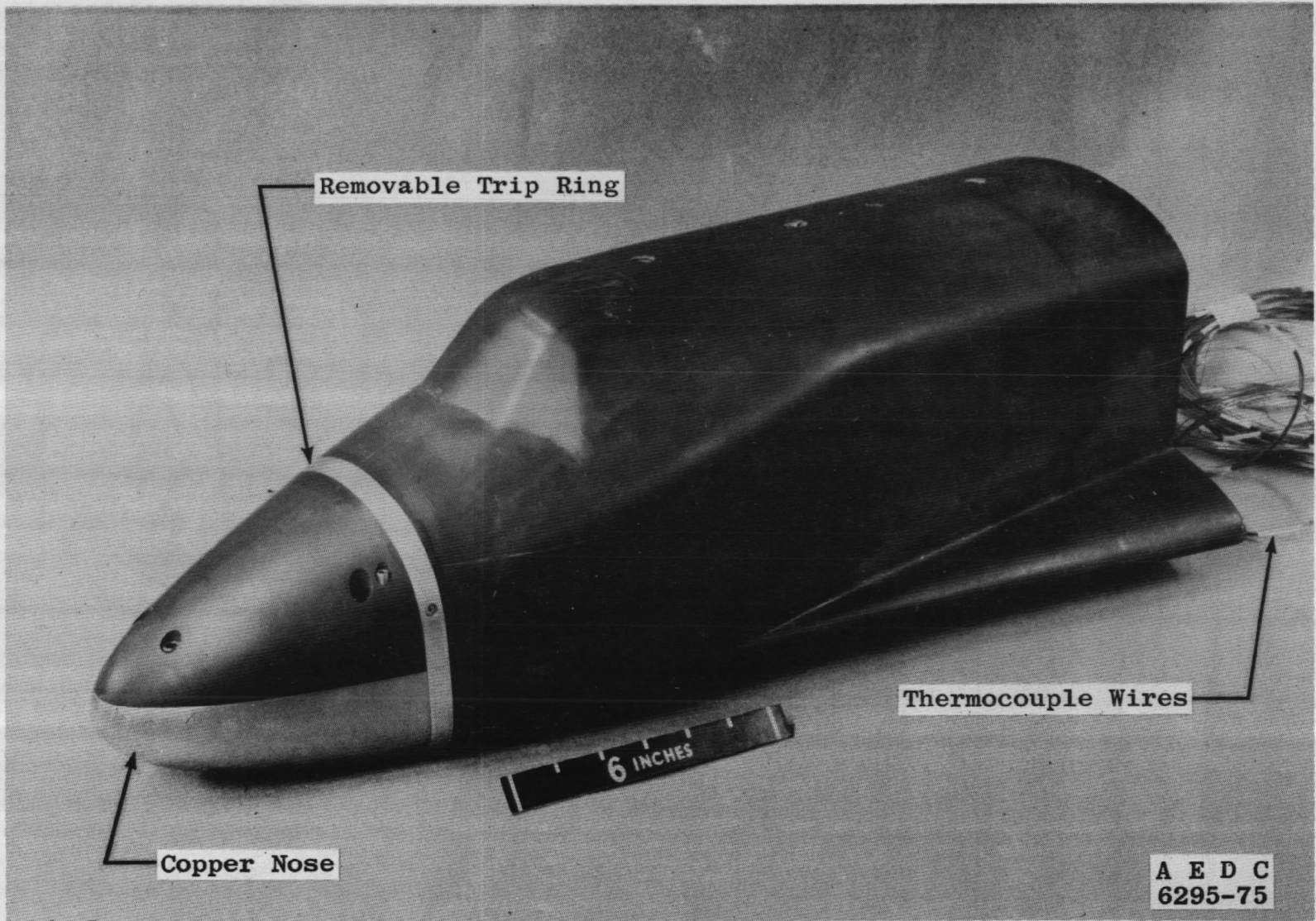
1. Sivells, James C. "Aerodynamic Design and Calibration of the VKF 50-Inch Hypersonic Wind Tunnels." AEDC-TDR-62-230 (AD299774), March 1963.
2. Martindale, W. R., Matthews, R. K., and Trimmer, L. L. "Heat-Transfer and Flow-Field Tests of the North American Rockwell/General Dynamics Convair Space Shuttle Configurations." AEDC-TR-72-169 (AD755354), January 1973.
3. Jones, Robert A. and Hunt, James L. "Use of Fusible Temperature Indicators for Obtaining Quantitative Aerodynamic Heat-Transfer Data." NASA-TR-R-230, February 1966.
4. Fay, J. A. and Riddell, F. R. "Theory of Stagnation Point Heat Transfer in Dissociated Air." Journal of the Aerospace Sciences, Vol. 25, No. 2, pp. 73-85, 121, February 1958.
5. Matthews, R. K. and Gilley, G. E. "Reduction of Photographic Heat-Transfer Rate Data at AEDC." AEDC-TR-73-90 (AD762928), June 1973.
6. Carter, L. D. and Kaul, C. E. "Heat-Transfer Tests on the Rockwell International Space Shuttle Orbiter with and without Simulated Protuberances." AEDC-TR-75-20 (ADA012876), July 1975.
7. Patankar, S. V. and Spaulding, D. B. Heat and Mass Transfer in Boundary Layers. CRC Press, Cleveland, 1968.
8. Mayne, A. W., Jr., and Dyer, D. F. "Comparisons of Theory and Experiment for Turbulent Boundary Layers on Simple Shapes at Hypersonic Conditions." in Proceedings of the 1970 Heat Transfer and Fluid Mechanics Institute, Stanford University Press, 1970.
9. Inouye, M., Rakich, J. V., and Lomax, H. "A Description of Numerical Methods and Computer Programs for Two-Dimensional and Axisymmetric Supersonic Flow over Blunt-Nosed and Flared Bodies." NASA TN D-2970, August 1965.



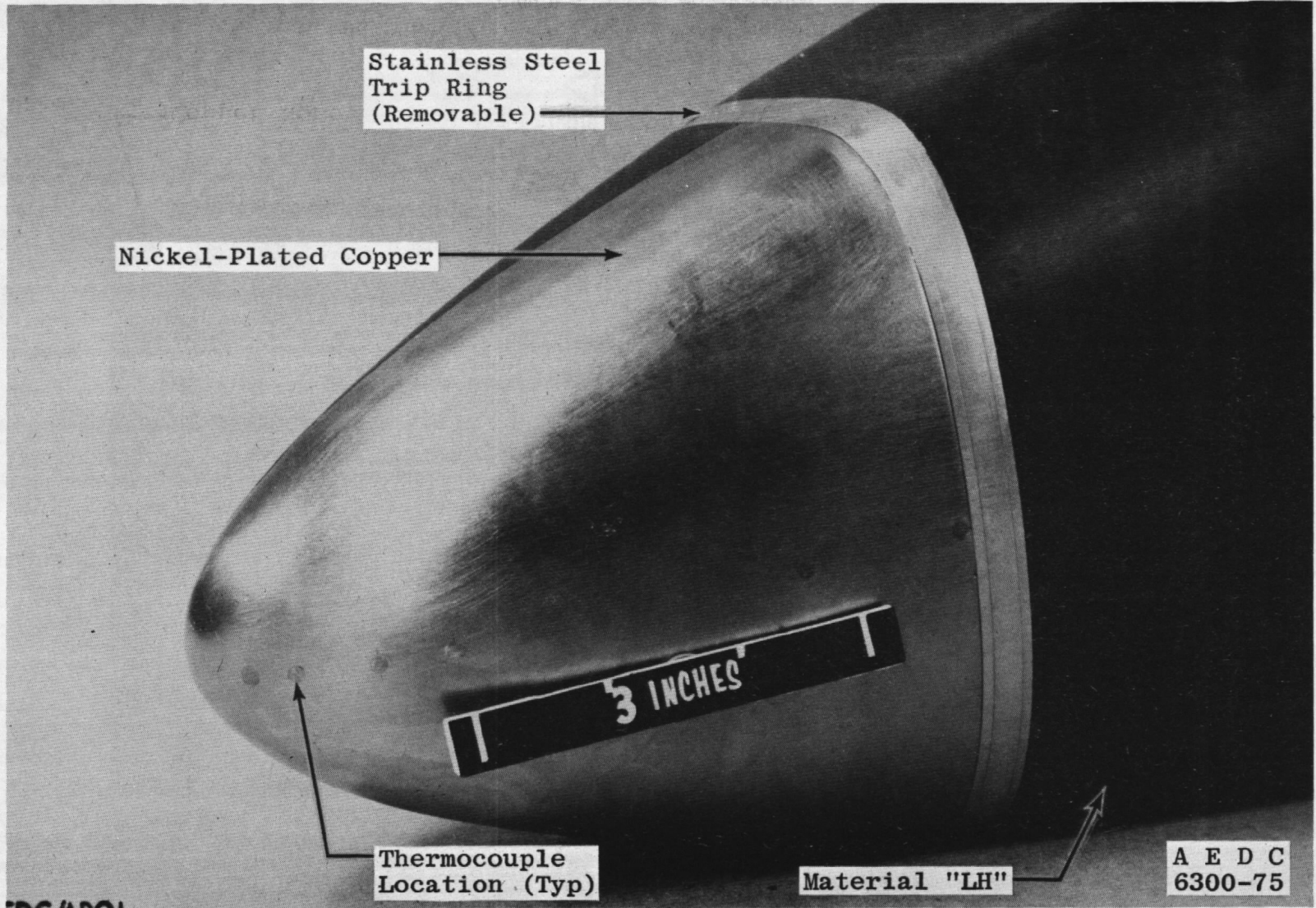
a. Tunnel assembly



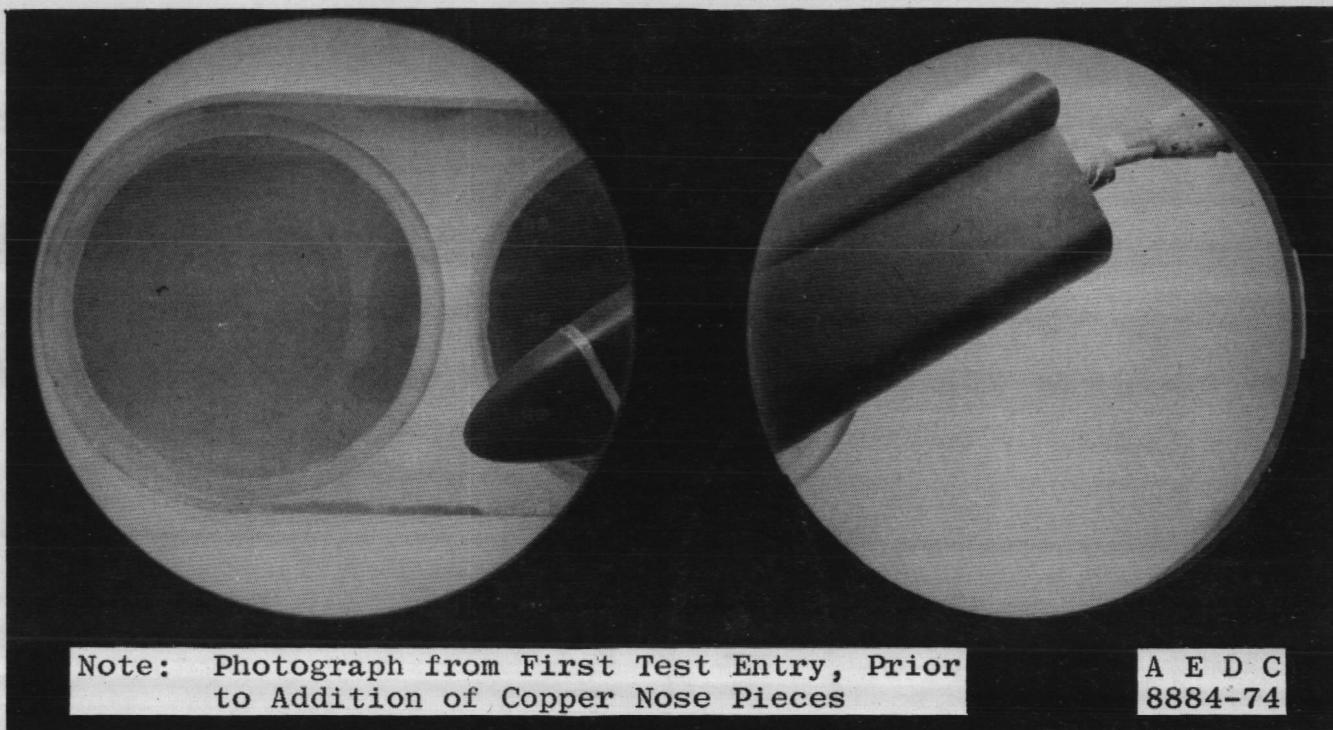
b. Tunnel test section  
Figure 1. Tunnel B.



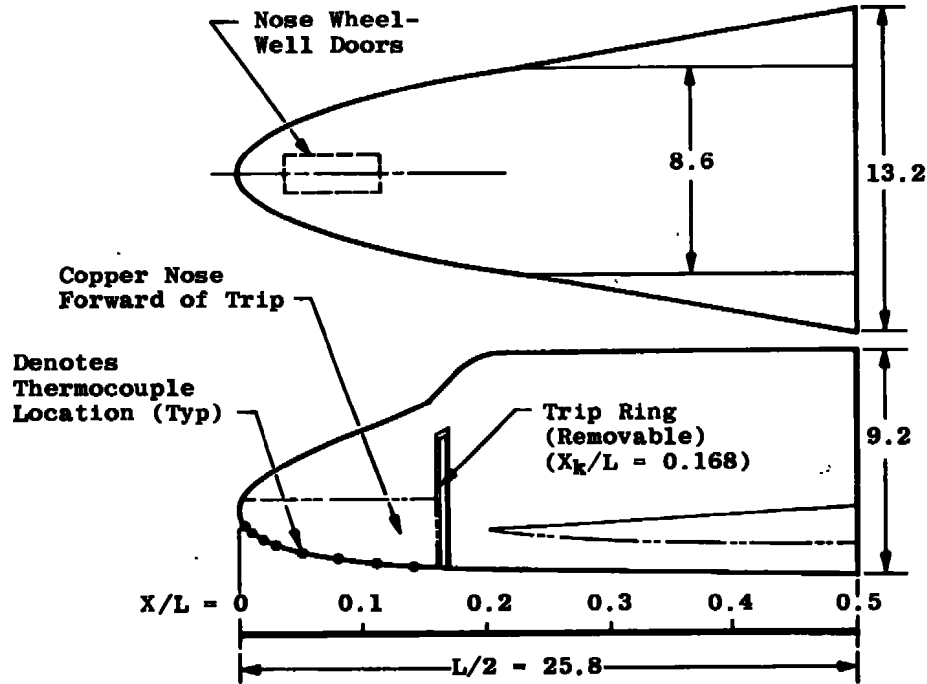
a. Mid-station ( $X_k/L = 0.110$ ) trip model, smooth trip ring installed  
Figure 2. Model photographs.



b. Detail of the nose  
Figure 2. Continued.



c. Mid-station ( $X_k/L = 0.110$ ) trip model installed in Tunnel B  
Figure 2. Concluded.



Notes:

1. All dimensions are in inches.
2. Trip ring location shown for the aft station trip model only.
3. Thermocouples shown are those of the aft station trip model only. The  $X/L$  stations are presented in the table below:

Trip Location		
$X_k/L = 0.052$	$X_k/L = 0.110$	$X_k/L = 0.168$
X/L Values of the Thermocouples		
0.005	0.005	0.005
0.010	0.010	0.010
0.020	0.020	0.020
0.030	0.030	0.030
0.045	0.050	0.050
---	0.080	0.080
---	0.103	0.110
---	---	0.140
---	---	0.162

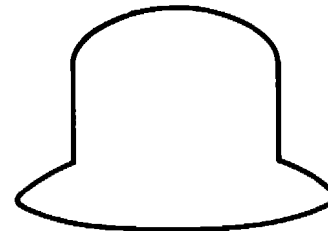


Figure 3. Sketch of the orbiter forebody models.

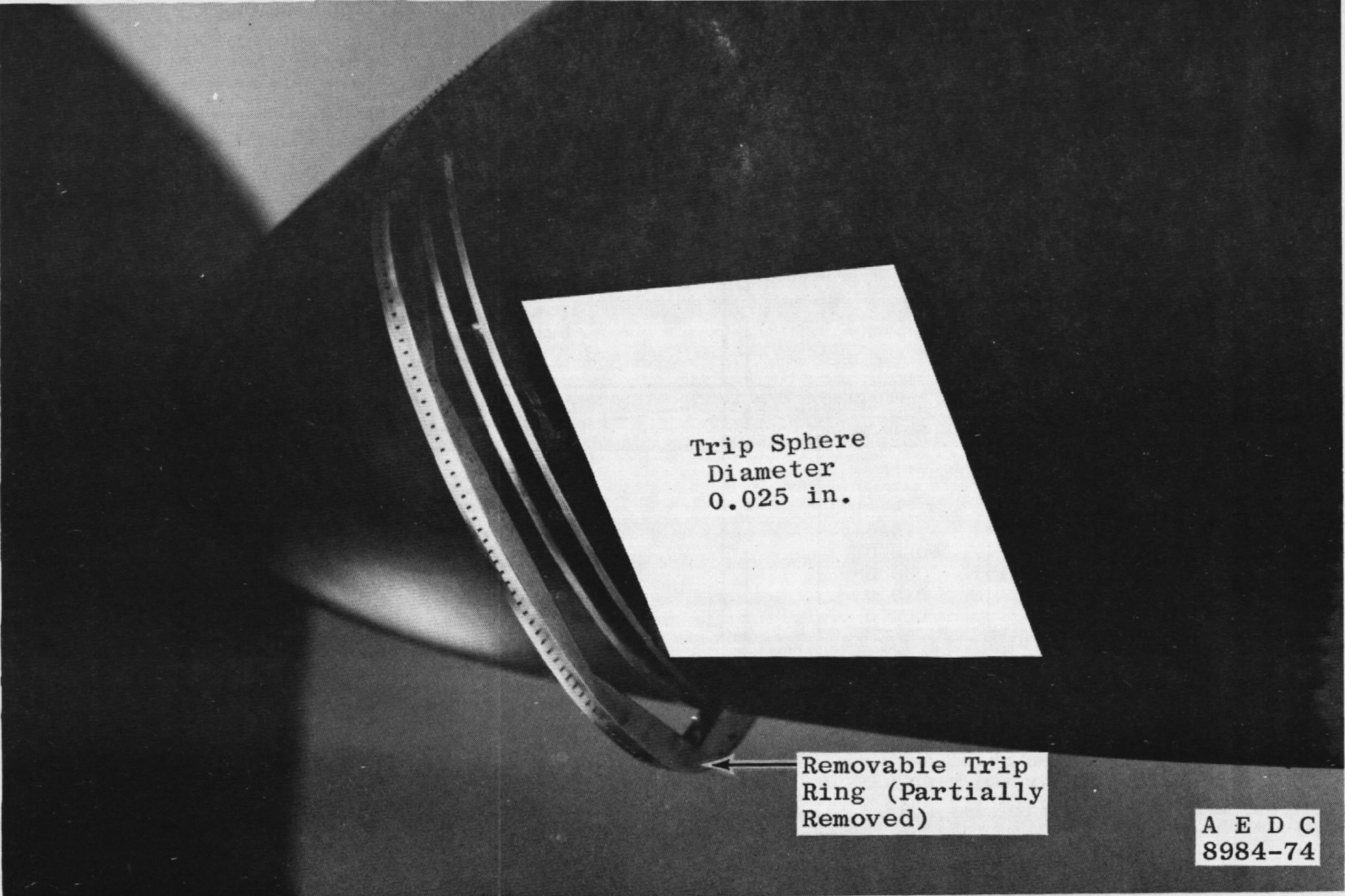


Figure 4. Trip ring photograph.

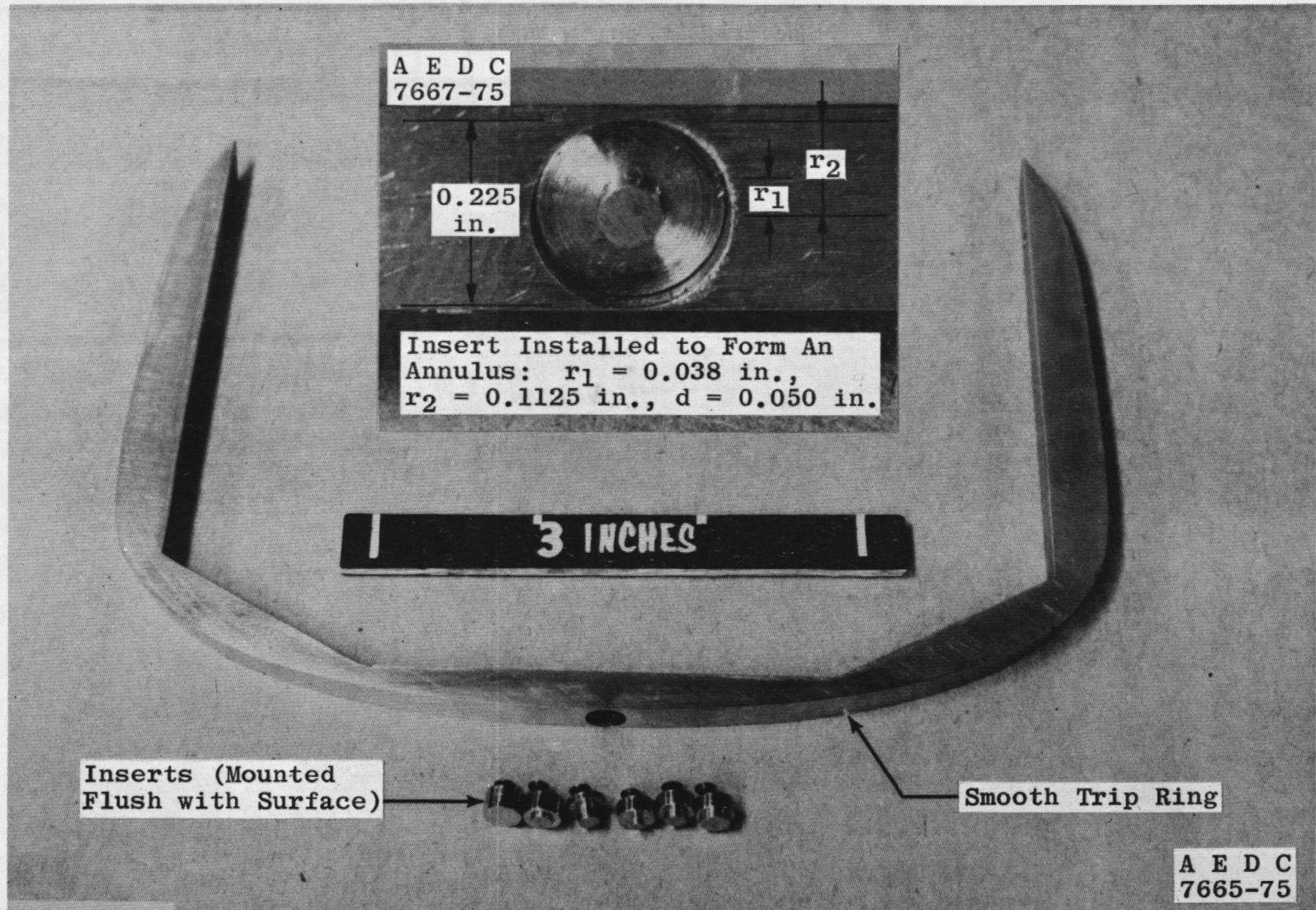


Figure 5. Photograph of the smooth trip ring modified to simulate the external tank attachment ring.



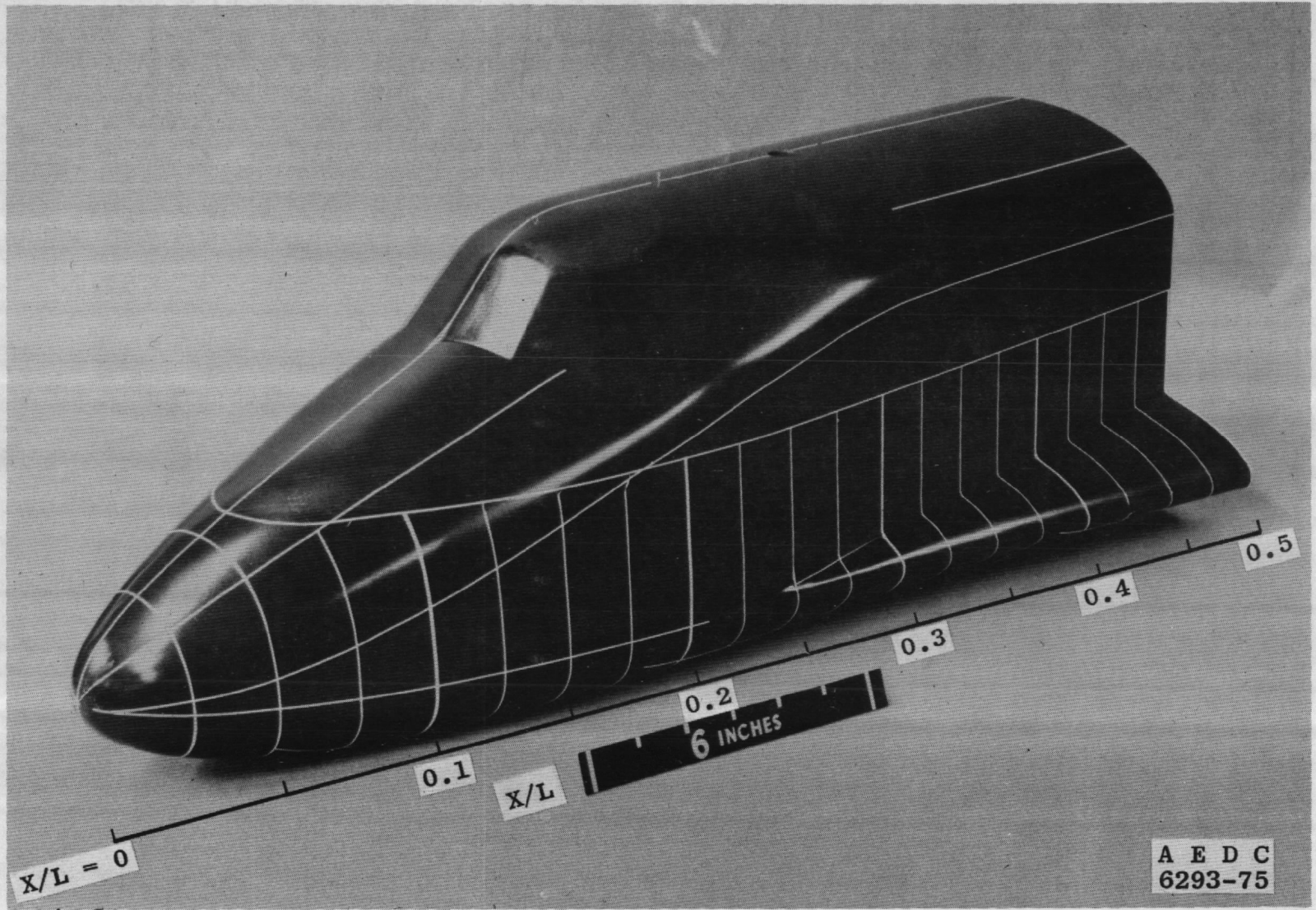
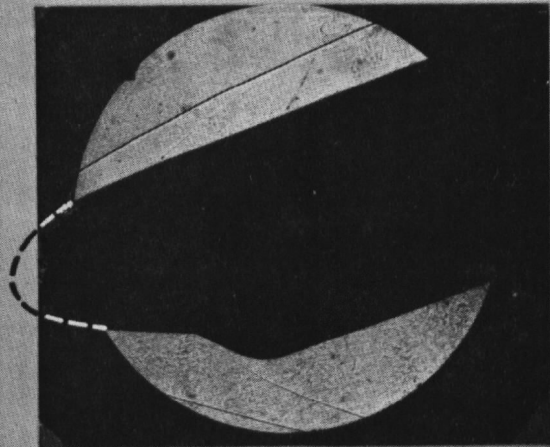


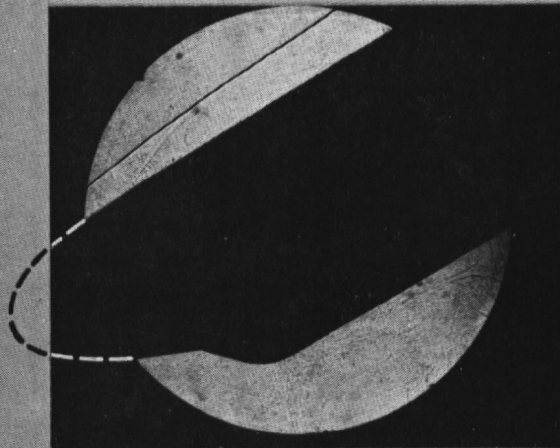
Figure 6. Photograph of the paint stripe model.

0383-10  
A T C  
A R D C

a.  $a = 20$  deg



b.  $a = 30$  deg



c.  $a = 40$  deg

Shock  
from  
Trip  
Spheres

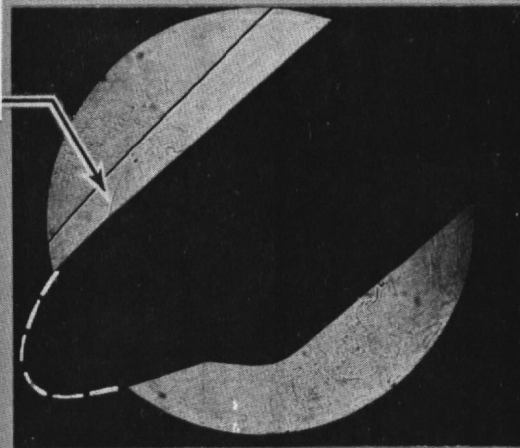
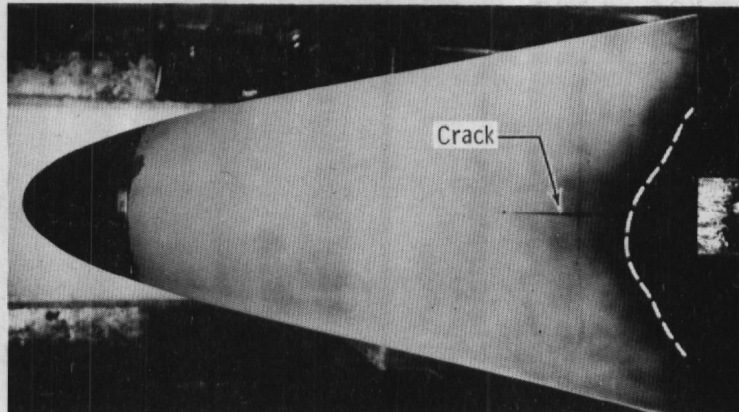


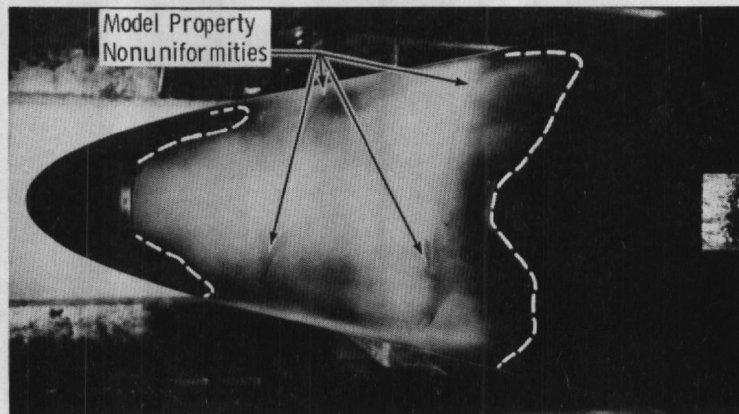
Figure 7. Typical shadowgraphs, 0.031-in.-diam spheres at  $X_k/L = 0.168$ ,  $Re_{\infty,L} = 6.5 \times 10^6$ .

Melt Line  
Value,  $h/h_{ref}$

0.27



0.14



0.09

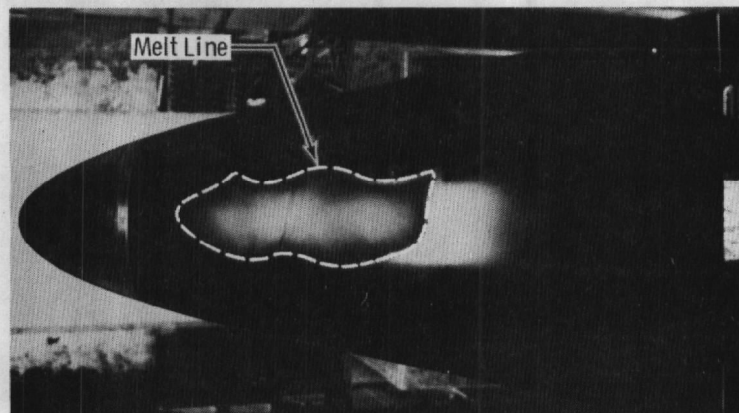
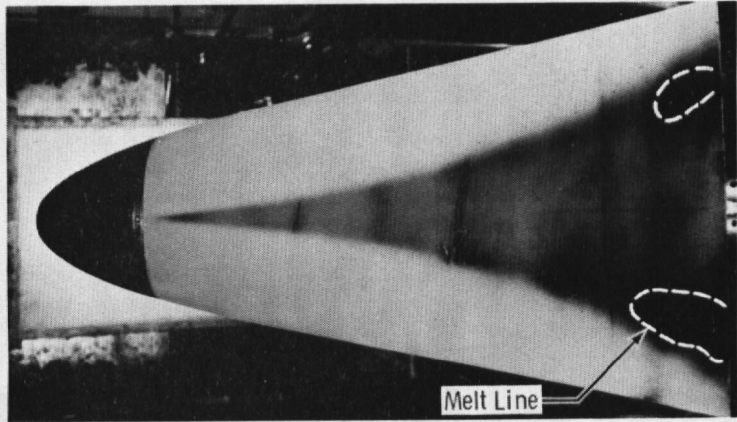


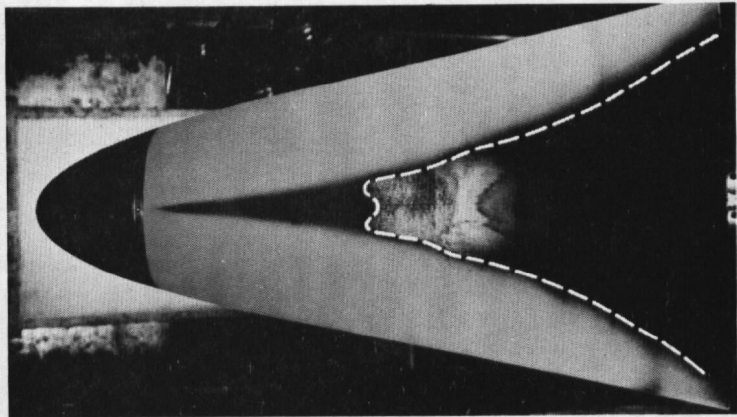
**Figure 8.** Phase-change paint photographs of the mid-station trip model with a smooth trip ring installed,  $Re_{cor,L} = 12.9 \times 10^6$ ,  $\alpha = 30$  deg.

Melt Line  
Value,  $h/h_{ref}$

0.32



0.29



0.22

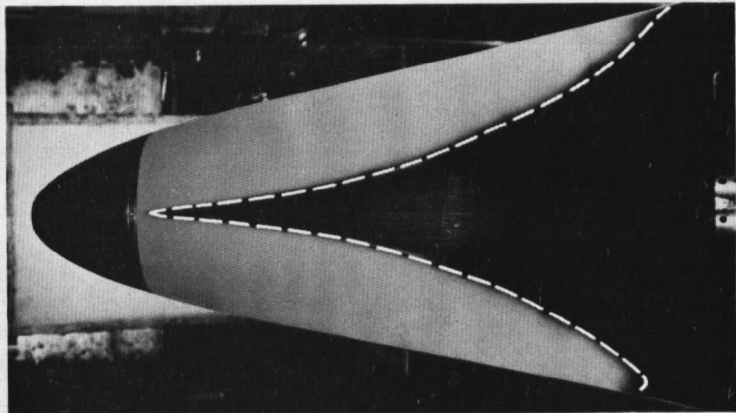
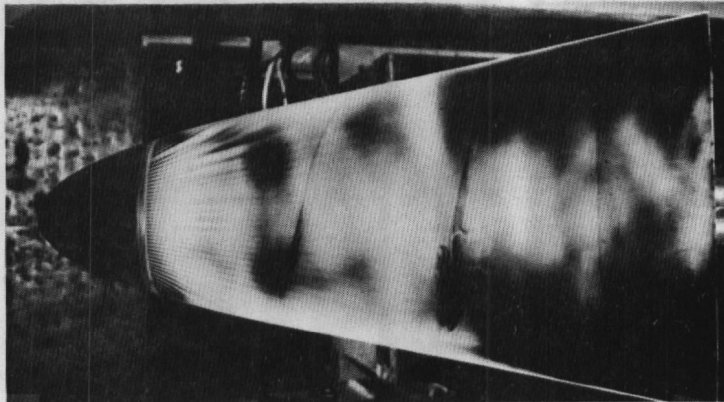


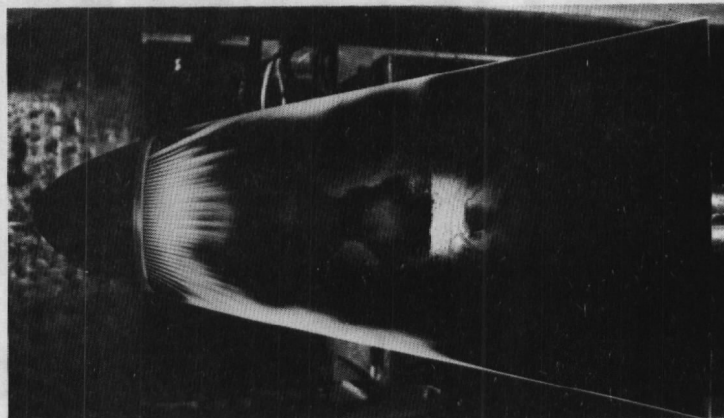
**Figure 9.** Phase-change paint photographs of an external tank attachment ring configuration ( $r_1 = 0.063$  in.,  $d = 0.050$  in.)  $Re_{\infty L} = 12.9 \times 10^6$ ,  $\alpha = 30$  deg.

Melt Line  
Value,  $h/h_{ref}$

0.24



0.22



0.19

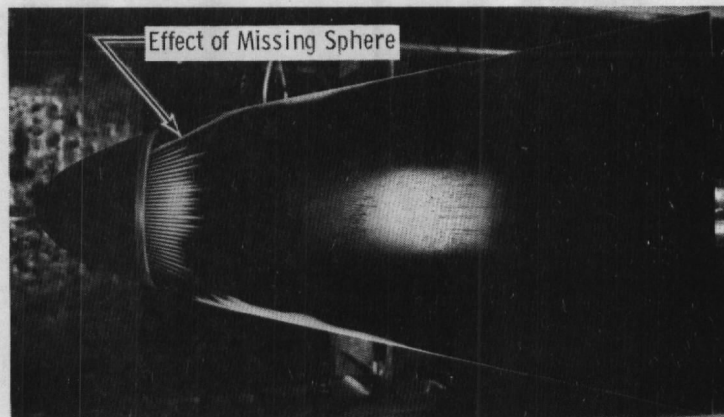
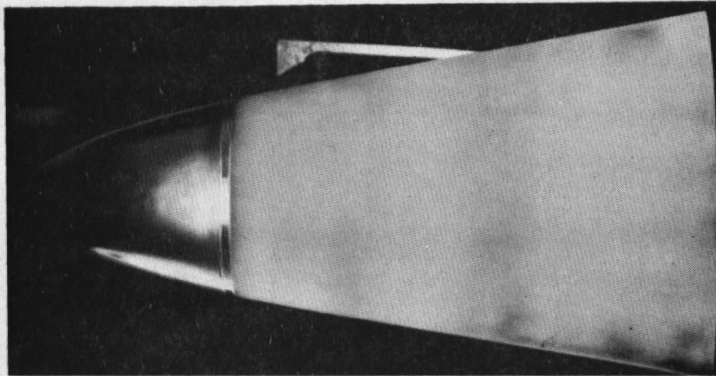


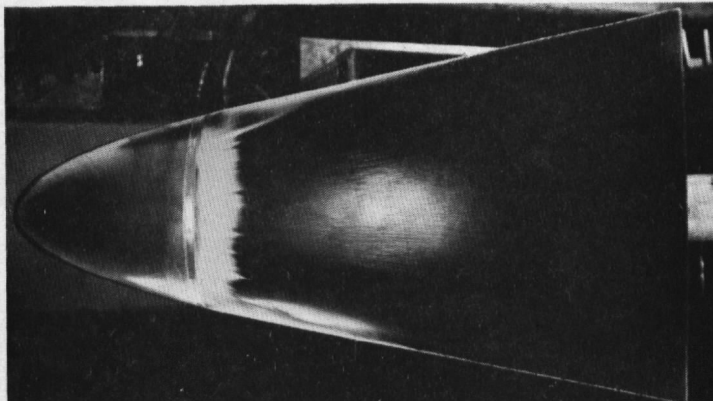
Figure 10. Phase-change paint photographs of a trip model, 0.031-in.-diam spheres at  $X_k/L = 0.110$ ,  $Re_{\infty,L} = 8.6 \times 10^6$ ,  $\alpha = 30$  deg.

$\alpha$ , deg

20


 $h/h_{ref} < 0.27$   
 (No Melt)

30



40

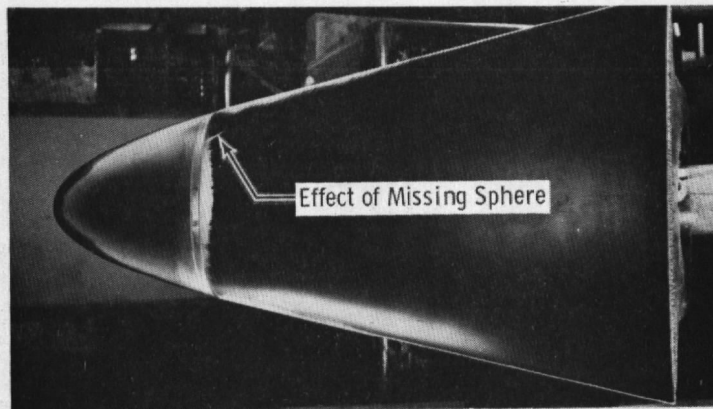
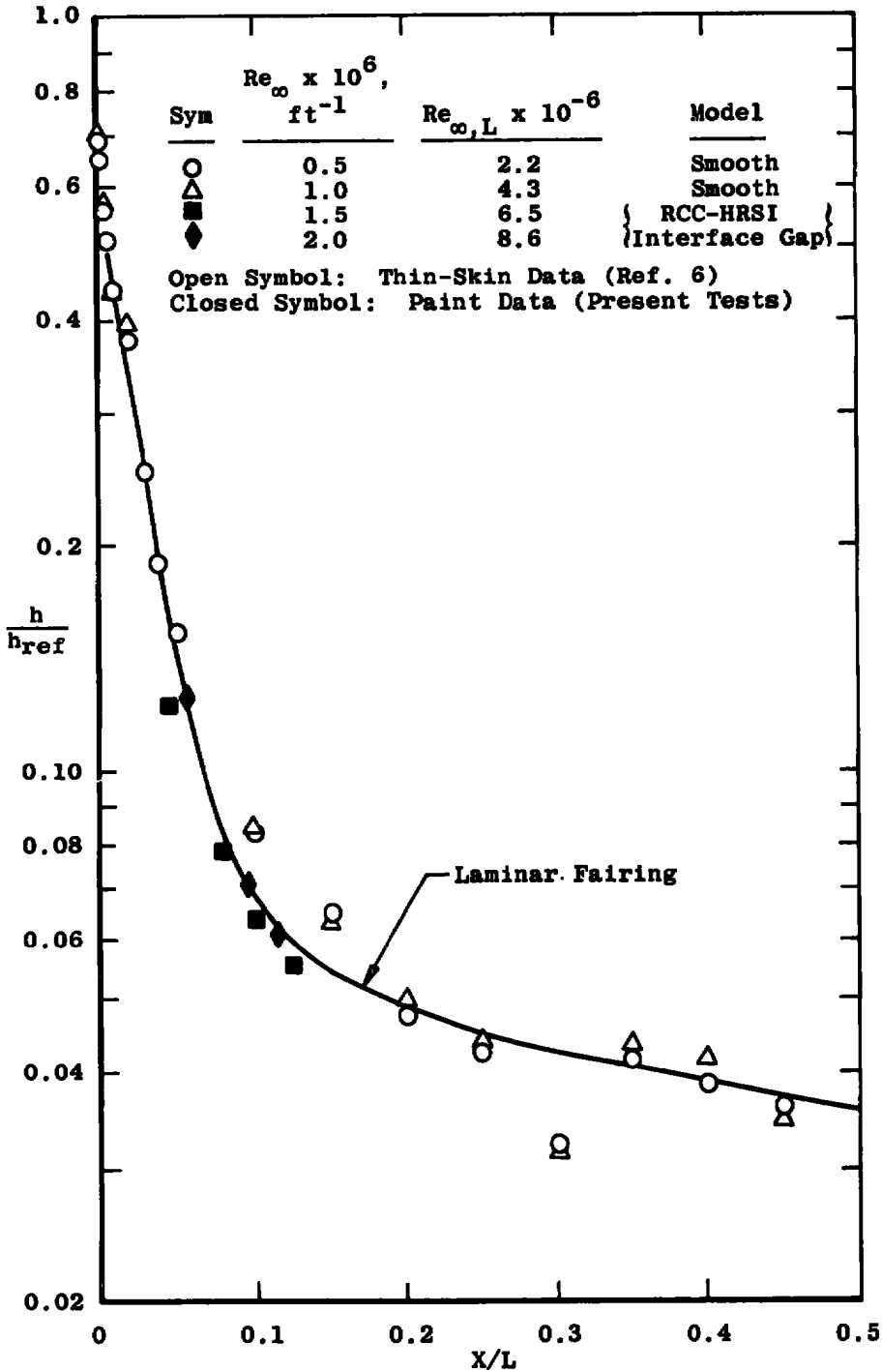
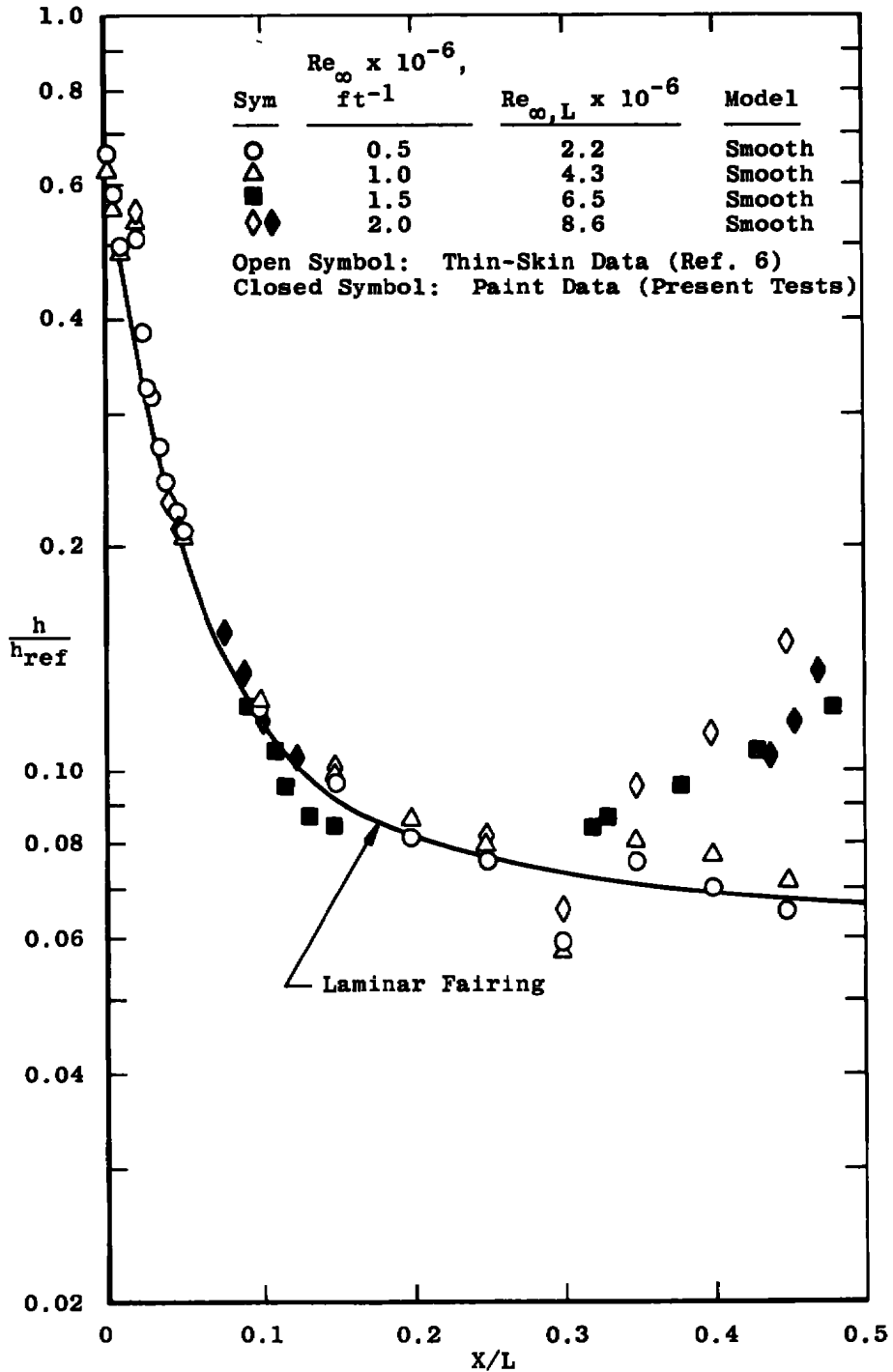


Figure 11. Photographs of the effect of angle of attack for a constant melt line heat-transfer coefficient,  $h/h_{ref} = 0.27$ , 0.020-in.-diam spheres at  $X_k/L = 0.168$ ,  $Re_{\infty,L} = 12.9 \times 10^6$ .



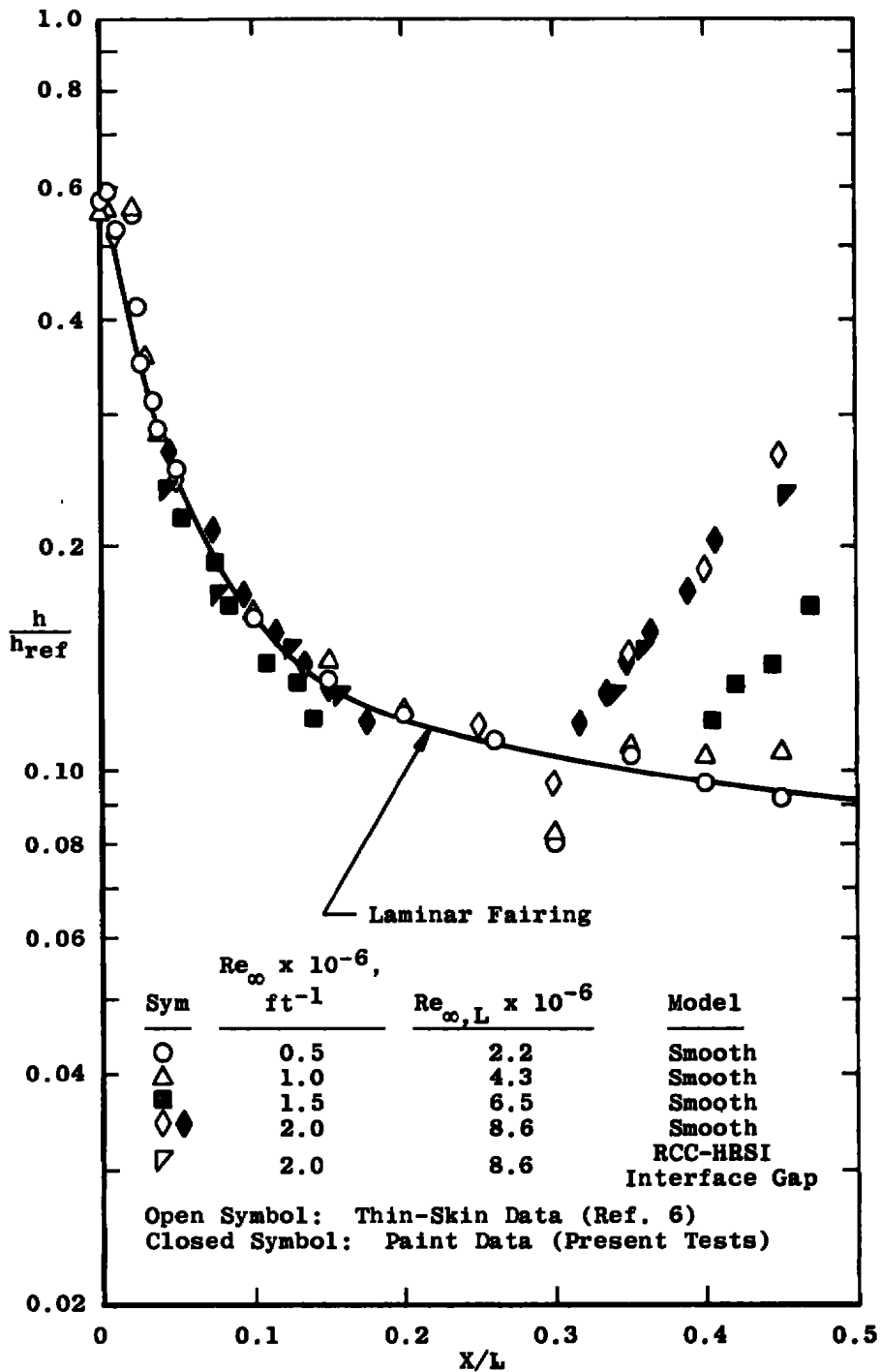
a.  $\alpha = 20$  deg

Figure 12. Determination of the laminar heat-transfer distribution along the windward centerline.



b.  $\alpha = 30$  deg  
 Figure 12. Continued.





c.  $\alpha = 40$  deg  
 Figure 12. Concluded.

Sym	$Re_{\infty,L} \times 10^{-6}$	Theoretical Curves	
		$Re_{\infty,L} \times 10^{-6}$	$T_w/T_o$
○●	4.4	4.4	0.52
△	5.4	8.6	0.58
□	6.5	15.1	0.65
◇	7.6		
▽	8.5		
◊	9.6		
◇	10.7		
○	12.9		

Solid Symbol: Test conditions were repeated using a lower paint temperature.

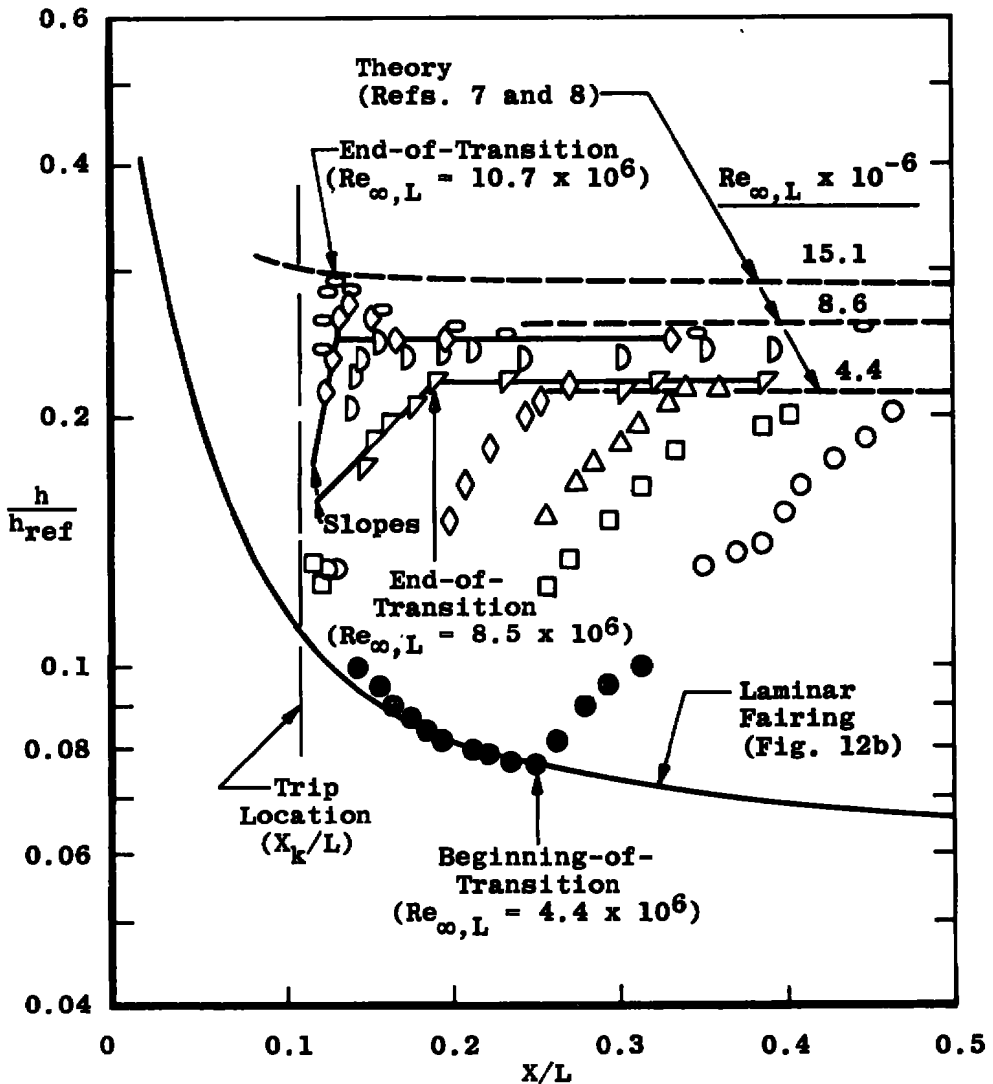


Figure 13. Effect of Reynolds number on the windward centerline heat-transfer distribution, 0.031-in.-diam spheres at  $X_k/L = 0.110$ ,  $\alpha = 30$  deg.

Sym

Data

- Trip Model,  $X_k/L = 0.110$ ,  $k_d = 0.031$  in.
- △▲ Smooth Model

Open Symbol: Thin-Skin Data (Ref. 6)

Closed Symbol: Paint Data (Present Tests)

Flagged Symbol: Theoretical Turbulent Level Used in Determining  $X_t/L$

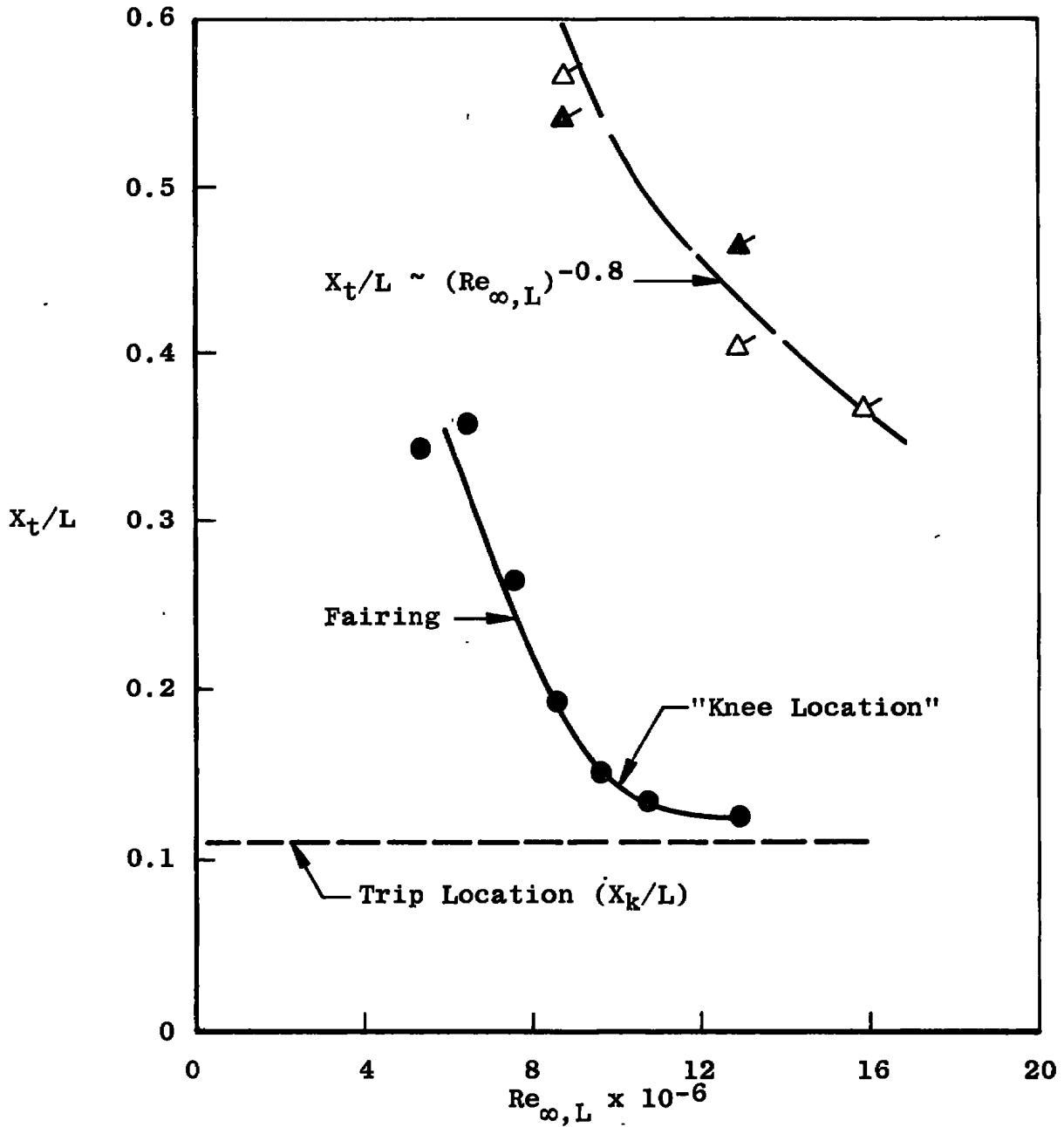


Figure 14. Determination of trip effectiveness, 0.031-in.-diam spheres at  $X_k/L = 0.110$ ,  $\alpha = 30$  deg.

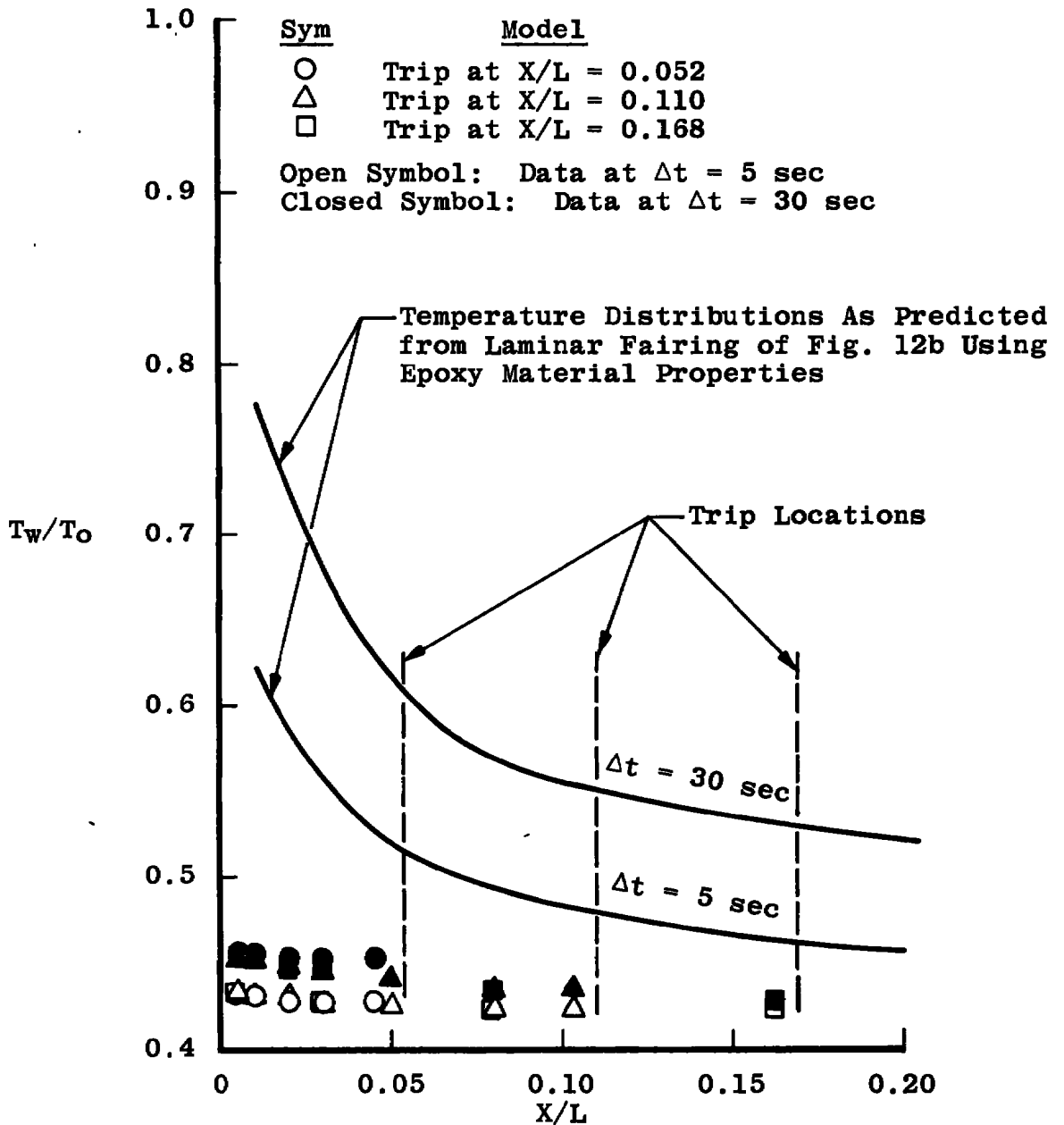


Figure 15. Effect of the copper nose on the windward centerline temperature distribution,  $Re_{\infty L} = 8.6 \times 10^6$ ,  $\alpha = 30$  deg.

Table 1. Trip Sphere Sizes Tested

Model Trip Location, $X_k/L$	Sphere Size, $k_d$ , in.					
	0.000	0.015	0.020	0.025	0.031	0.039
0.052	x	x	x	x		
0.110	x	x	x	x	x	x
0.168	x		x	x	x	

Table 2. External Tank Attachment Ring Dimensions

Insert No.	Annulus Dimensions, in.		
	$r_1$	$r_2$	d
1	0.088	0.113	0.050
2	0.063	↓	0.050
3	0.038		0.050
4	0.063		0.100
5	0.063		0.025
6	0.113		0.000

Table 3. Summary of Test Data

Configuration	$\alpha$ , deg	Spherical Trip Diameter, $k_d$ , in.	$Re_\infty \times 10^{-6}$ , ft <sup>-1</sup>												
			0.75	1.00	1.25	1.50	1.75	2.00	2.25	2.50	2.75	3.00	3.25	3.50	3.75
Smooth	20														
	30					x			x						
	40				x	x			x						
Landing Gear Door	20										x	x	x		
	30				x	x	x		x		x				
	40			x	x	x			x						
RCC-HRSI Interface Gap	20					x			x	x			x		x
	30					x			x	x			x		x
	40					x			x		x		x		x
Trip at $X/L = 0.052$	20	0.000													
	30	↓													
	40	↓				x			x		x		x		
	20	0.015							x	x	x	x	x	x	
	30	↓							x	x	x	x	x	x	
	40	↓							x	x	x	x	x	x	
	20	0.020													
	30	↓				x	x		x	x	x	x			
	40	↓				x	x	x	x	x	x				
	20	0.025													
	30	↓				x	x	x	x	x	x				
	40	↓				x	x	x	x	x	x				

Table 3. Continued

Configuration	$\alpha$ , deg	Spherical Trip Diameter, $k_d$ , in.	$Re_\infty \times 10^{-6}$ , $ft^{-1}$															
			0.75	1.00	1.25	1.50	1.75	2.00	2.25	2.50	2.75	3.00	3.25	3.50	3.75			
Trip at $X/L = 0.110$	20	0.000 ↓																
	30								x		x							x
	40								x		x							x
	20	0.015 ↓									x	x	x	x	x	x	x	x
	30								x	x	x	x	x	x	x	x	x	x
	40								x	x	x	x	x	x	x	x	x	x
	20	0.020 ↓									x	x	x	x	x	x	x	
	30					x	x	x	x	x	x	x	x	x	x	x	x	
	40				x	x	x	x	x	x	x	x	x	x	x	x	x	
	20	0.025 ↓																
	30					x	x	x	x	x	x	x						
	40			x	x	x	x	x	x	x	x	x						
20	0.031 ↓										x	x	x	x	x	x		
30				x	x	x	x	x	x	x	x	x	x	x	x	x		
40			x	x	x	x	x	x	x	x	x	x	x	x	x	x		
20	0.039 ↓																	
30				x	x	x	x	x	x	x	x							
40		x	x	x	x	x	x	x	x	x								
Trip at $X/L = 0.168$	20	0.000 ↓																
	30										x							
	40							x			x							
	20	0.020 ↓									x	x	x	x	x	x	x	
	30							x	x	x	x	x	x	x	x	x	x	
	40					x	x	x	x	x	x	x	x	x	x	x	x	
	20	0.025 ↓																
	30							x	x	x	x	x	x	x	x	x	x	
	40		x	x	x	x	x	x	x	x	x	x	x	x	x	x	x	
	20	0.031 ↓																
	30							x	x	x	x	x	x	x	x	x	x	
	40				x	x	x	x	x	x	x	x	x	x	x	x	x	

Table 3. Concluded

Configuration	$\alpha$ , deg	Annulus		$Re_{\infty} \times 10^{-6}$ , $ft^{-1}$												
		$r_1$ , in.	$d$ , in.	0.75	1.00	1.25	1.50	1.75	2.00	2.25	2.50	2.75	3.00	3.25	3.50	3.75
ET Attachment Ring	30	0.088	0.050								x	x	x	x	x	x
	35	↓	↓													
	40	↓	↓													
	30	0.063	0.050					x	x	x	x	x	x			
	35	↓	↓			x	x	x	x	x	x					
	40	↓	↓		x	x	x	x	x	x						
	30	0.038	0.050				x	x	x	x	x					
	35	↓	↓													
	40	↓	↓													
	30	0.063	0.100						x	x	x	x		x		
	35	↓	↓													
	40	↓	↓													
	30	0.063	0.025									x	x	x	x	x
	35	↓	↓													
	40	↓	↓													
	30	0.113	0.000							x		x		x		
	35	↓	↓							x		x				
	40	↓	↓							x		x				



**Table 4. Model Material Thermophysical Properties**

Models	$T_{pc},$ $^{\circ}F$	$k,$ Btu/ft-sec- $^{\circ}R$	$c_p,$ Btu/lbm- $^{\circ}R$	$w,$ lbm/ft <sup>3</sup>	$\sqrt{wc_p k}$ Btu/ft <sup>2</sup> - $^{\circ}R$ -(sec <sup>1/2</sup> )
A	150	0.0000750	0.271	125.4	0.0505
	169	0.0000750	0.282	↓	0.0515
	175	0.0000750	0.285		0.0518
	200	0.0000747	0.299		0.0529
	250	0.0000742	0.326		0.0551
	275	0.0000739	0.338		0.0560
	300	0.0000736	0.350		0.0568
	350	0.0000728	0.367		0.0579
	388	0.0000725	0.375		0.0584
	400	0.0000722	0.378		0.0585
	413	0.0000722	0.378		0.0585
B	150	*	*		*
	169				0.0569
	175				0.0573
	200				0.0586
	250				0.0617
	275				0.0627
	300				0.0636
	350				0.0652
	388				0.0659
	400				0.0660
	413				0.0660

Models: A ~ Smooth and Landing Gear Door

B ~ Trip ring models and RCC-HRSI Gap Model

\* Material properties were furnished as the lumped parameter,  $\sqrt{wc_p k}$ , by the manufacturer.

## NOMENCLATURE

$c_p$	Specific heat of model material, Btu/lbm-°R
$d$	Depth of the ET attachment ring annulus, in.
$h$	Heat-transfer coefficient, $\dot{q}/(T_o - T_w)$ , Btu/ft <sup>2</sup> -sec-°R
$k$	Model material conductivity, Btu/ft-sec-°R
$k_d$	Spherical roughness element diameter, in.
$L$	Scaled axial length of Orbiter, 51.6 in.
$M$	Mach number
$p_o$	Stilling chamber pressure, psia
$q$	Heat-transfer rate, Btu/ft <sup>2</sup> -sec
$Re_\infty$	Free-stream unit Reynolds number, ft <sup>-1</sup>
$Re_{\infty L}$	Free-stream Reynolds number based on $L$
$r_1$	Inner radius of the ET attachment ring annulus (see Fig. 5), in.
$r_2$	Outer radius of the ET attachment ring annulus, 0.1125 in.
$T$	Temperature, °F or °R as noted
$\Delta t$	Time increment that model has been exposed to uniform flow, sec
$w$	Model material density, lbm/ft <sup>3</sup>
$X$	Axial distance from model nose, in.
$X_k$	Axial distance from model nose to center of roughness element, in.
$X_t$	Axial distance from model nose to end-of-transition, in.
$\alpha$	Angle of attack, deg
$\beta$	Semi-infinite heating equation parameter, $h\sqrt{\Delta t}/\sqrt{wc_p k}$

**SUBSCRIPTS**

<b>aw</b>	<b>Adiabatic wall conditions</b>
<b>i</b>	<b>Initial conditions</b>
<b>o</b>	<b>Stilling chamber conditions</b>
<b>pc</b>	<b>Phase change</b>
<b>ref</b>	<b>Heat-transfer parameter based on Fay-Riddell theory and a 1-ft nose radius scaled down to the model scale (i.e., 0.04 ft)</b>
<b>w</b>	<b>Wall conditions</b>
<b>∞</b>	<b>Free-stream conditions</b>